Physics – Uspekhi **64** (2) 109 – 140 (2021)

REVIEWS OF TOPICAL PROBLEMS PACS numbers: 02.70.Jn, 64.70.fm, 68.03.Fg

Heat and mass transfer at condensate–vapor interfaces

A P Kryukov, V Yu Levashov, V V Zhakhovskii, S I Anisimov

DOI: https://doi.org/10.3367/UFNe.2020.04.038749

Contents

Abstract. Evaporation and condensation processes are intensely used in various fields of technology. Efforts to understand the features of film boiling of various liquids, primarily superfluid helium, inevitably lead to studying the strongly nonequilibrium processes of heat transfer from the heating surface through the vapor to the condensed phase. Theoretical studies of evaporation and condensation of single-component substances are briefly reviewed. Corresponding experimental data are analyzed and compared with calculations. We explore the important, yet unresolved and actively studied problems of condensation from vapor–gas media, the formulation of boundary conditions, and the application of molecular dynamics and kinetic theory methods to the study of heat and mass transfer at phase interfaces.

Keywords: evaporation, condensation, interphase transition layer, determination of phase interface, strongly nonequilibrium processes, gas–vapor mixture, liquid–vapor saturation curve, experiments on high-rate evaporation–condensation, superfluid helium, evolution of distribution functions in interphase, molecular-kinetic theory, molecular dynamics simulation

A P Kryukov [1, a], **V Yu Levashov** [2, b], **V V Zhakhovskii** [3, c], **S I Anisimov** [4]
[1] National Research University Moscow Power Engineering Institute, ul. Krasnokazarmennaya 14, 111250 Moscow, Russian Federation
[2] Lomonosov Moscow State University, Institute of Mechanics, Michurinskii prosp. 1, 119192 Moscow, Russian Federation
[3] Dukhov Research Institute of Automatics, ul. Sushchevskaya 22, 127055 Moscow, Russian Federation
[4] Landau Institute for Theoretical Physics, Russian Academy of Sciences, prosp. Akademika Semenova 1A, 142432 Chernogolovka, Moscow region, Russian Federation
E-mail: [a] KryukovAp@mail.ru, [b] vyl69@mail.ru, [c] 6asi1z@gmail.com

Received 29 December 2019, revised 2 April 2020
Uspekhi Fizicheskikh Nauk **191** (2) 113 – 146 (2021)
Translated by M Zh Shmatikov

1. Introduction

Almost 140 years have passed since the publication of Hertz's pivotal theoretical study [1] on evaporation. A great deal of research experience has been accumulated since then, which should be considered to determine the current state of the problem and the prospects for development in this field. The processes of evaporation and condensation are at present theoretically studied using the methods of continuum mechanics (CM), molecular kinetic theory (MKT), and molecular dynamics modeling (MD).

Owing to the relative simplicity of the equations of continuum mechanics, well-developed analytical and numerical methods for their solution, and the available computer facilities, CM methods are very attractive. However, it is not possible in CM-based approaches to determine near the interface the velocity of the vapor produced as a result of evaporation. This velocity is usually found, using the constancy of the energy flux in the stationary evaporation mode and disregarding the kinetic energy of the vapor, by dividing the specific heat flux supplied to the interface by the latent heat of vaporization and the equilibrium density of saturated vapor that corresponds to the interface temperature on the liquid–vapor equilibrium line. However, this approach is not always justified for the following reasons.

First, the vapor density near the interface at high intensities can significantly differ from that of saturated vapor. Second, the heat flux supplied to the interface may not be known in advance. For example, consider a solid or liquid in an environment of its own vapor with a given pressure. Assume that the condensed medium is affected by

thermal radiation, which, in general, is quite strong. It is required in realistic conditions that the temperature of the evaporation surface not exceed a certain value. What is the maximum thermal load that corresponds to this value in a stationary mode? The process develops as follows. Due to the increase in the interface temperature, part of the supplied heat is spent on heating the body and is removed from the surface into the bulk of the medium due to thermal conductivity and, in the case of a liquid medium, possible convection. Calculation of this component is not a challenging problem.

The rest of the total heat flux causes evaporation of the substance. Each component of the heat supplied depends on the surface temperature. It is clear that a unique determination of all parts of the heat flux is only possible if the relationship between this temperature and the flux of the evaporated material is known.

An example of using the system of CM conservation equations is the problem of evaporation from one surface and condensation of evaporated matter on another surface located at a certain distance from the first one, which was explored in 1952 by M Plesset [2]. However, it turns out that an additional relation is needed to close this system. As such, the Hertz–Knudsen formula was taken, which makes it possible under certain assumptions to find the mass flux density of the evaporating substance.

2. Description of evaporation and condensation using methods of molecular kinetic theory

2.1 Initial stage of exploration. Linear theory

The exploration of evaporation and condensation within the molecular kinetic theory is divided into stages, each of which is characterized by a certain level of development of the kinetic theory.

The study was carried out at an early stage using an elementary MKT, and later on the basis of conservation equations and specification of a distribution function of some known form. Hertz was the first to investigate evaporation and condensation using MKT approaches [1] (1882). Summarizing the results of his research, Hertz came to the following seminal conclusion: "For each substance, there is a maximum evaporation rate, which only depends on the surface temperature and the properties of the given substance. The maximum evaporation rate (by which we mean the number of molecules that evaporate per unit surface per unit time) can never exceed that of vapor molecules hitting the condensate surface in equilibrium." Therefore, the upper limit of the mass flux density $j_{\max}$ is

$$j_{\max} = \frac{V}{4} m n_{\mathrm{s}} = \frac{V}{4} \rho_{\mathrm{s}} ,$$

where V is the arithmetic mean velocity of the vapor molecules, $V = \sqrt{8RT_{\mathrm{s}}/\pi}$, R is the individual gas constant, ρ_{s} is the vapor density, which corresponds along the saturation line to the temperature of the interface surface T_{s}, $\rho_{\mathrm{s}} = m n_{\mathrm{s}}$, n_{s} is the number of saturated vapor molecules per unit volume (numerical density), and m is the mass of the molecule. In conducting experiments on the evaporation of mercury, Knudsen [3] concluded in 1915 that the evaporation rate at $T_{\mathrm{s}} \approx T_{\infty}$ is determined by the formula

$$j_{\mathrm{e}} = \beta \sqrt{\frac{RT_{\mathrm{s}}}{2\pi}} (\rho_{\mathrm{s}} - \rho_{\infty}) , \qquad (1)$$

where ρ_{∞} is the vapor density at a distance from the phase boundary — large compared to the average mean free path of vapor molecules.

Knudsen's study is of special significance, because it introduces the concept of evaporation–condensation coefficient β: the evaporation coefficient was defined as the ratio of the flow of molecules that escape from the liquid to the positive flow of molecules from the surface at liquid–vapor equilibrium. The latter flow is determined by the distribution of positive velocities obtained from the Maxwell distribution with zero transfer velocity, the temperature of the interphase surface, and the density that corresponds to this temperature on the saturation line, while the condensation coefficient determines the proportion of molecules that remain on the surface or, in other words, the molecules that condense, to the number of molecules incident on that surface. It should be noted that, at or near equilibrium, these coefficients are equal to each other [4], which allows the term 'condensation coefficient' to be used.

Equation (1) is one of the forms in which the famous Hertz–Knudsen formula may be represented. It was assumed in deriving this formula that far from the interface the distribution function (DF) is a four-moment double-sided Maxwellian distribution with the parameters ρ_{s}, T_{s} and ρ_{∞}, T_{∞}. This distribution is close at low vapor flow rates to the equilibrium Maxwellian one, but as the intensity of evaporation or condensation increases, the DF is increasingly different from this function.

Risch [5] and Crout [6] published in the mid-1930s their studies in which attempts were made to analyze the vapor flow in a more accurate way; the derivation of the Hertz–Knudsen formula is based on two assumptions that, strictly speaking, are unrealistic, especially if the rates of evaporation or condensation are high, and if the characteristic dimensions of the vapor regions under study L are much larger than the average mean free path of vapor molecules l (continuous flow regime at low Knudsen numbers, $\mathrm{Kn} = l/L \ll 1$). The first of these assumptions is that the vapor is macroscopically immobile at the interface. The second assumption is that the velocity distribution function of the molecules both flying away from the interface and moving in the opposite direction, i.e., to the boundary, is half-Maxwellian near the interface.

An attempt to take into account the motion of a vapor flow during condensation was first made in 1933 by Risch [5], who assumed that evaporation and condensation are independent of each other. Risch also conjectured in analyzing microscopic characteristics that the absolute values of the velocities of all molecules are equal to each other in the intrinsic coordinate system of a moving flow, $|\mathbf{V}| = \sqrt{2RT}$, while the directions of their motion at a solid angle of 4π are equally probable. In determining the flow of molecules that impinge upon the surface, the velocity at which the molecule hits the interface is determined by the sum of the vectors $\mathbf{V}$ and $\mathbf{u}$, where $\mathbf{u}$ is the mass velocity of the condensed vapor. According to the modern kinetic theory, such an approach, although it takes into account macroscopic motion at the interface, is rough due to the overly simplified form of the assumed molecular velocity distribution function. However, it must be emphasized that this roughness is much less significant compared to the macroscopic motion of the vapor being taken into account.

Of great interest is the method to calculate the evaporation process developed in the study by P Crout [6] in 1936, where the analysis is based on an ellipsoidal distribution

function that transforms into a Maxwellian distribution when leaving the Knudsen layer, $L \sim l$. Although the Boltzmann equation was not solved in Crout's work, this study remains of interest at the present time, since it provides an example of how a clear understanding of the physical characteristics of evaporation makes it possible to determine in an approximately correct way both the velocity distribution function of molecules and the basic regularities of this process.

Mentioned next in chronological order should be the monograph of 1953 by R Schrage [7], in which attempts were made to construct a 'simple' theory of mass transfer through an interface. In summarizing the analysis of the explorations made at this stage, it should be emphasized that, in this group of studies, the most physically substantiated and relatively strictly constructed is one of the early studies of evaporation carried out by P Crout in 1936.

The next stage in the exploration of evaporation and condensation dates back to the 1960s, when the rapid pace of development of the dynamics of rarefied gases and the needs of modern technology led to the emergence of more rigorous calculation methods based on an exact or approximate solution of the kinetic equation. It was at that time that the linear theory was developed. It was initiated by the studies by Kucherov and Rikenglaz [8, 9], in which the above-mentioned features were taken into account. The authors of [8, 9] assumed a form of the velocity distribution function of molecules near the interphase surface that differs from that employed in deriving the Hertz–Knudsen formula. Namely, they assumed that the DF for the molecules that move to this surface is the same as for the negative half-space of velocities at a considerable distance from the interface. They determined then the expression for the mass flux that follows from the definition and utilized these DFs to obtain a result that differs by a factor of two from the mass flux calculated using the Hertz–Knudsen formula:

$$j_e = \rho_\infty u_\infty \approx 2\sqrt{\frac{RT_s}{2\pi}}\,(\rho_s - \rho_\infty)\,.$$

Further, according to Kucherov and Rikenglaz [9], for an arbitrary value of the condensation coefficient β,

$$j_e = \frac{2\beta}{2-\beta}\sqrt{\frac{RT_s}{2\pi}}\,(\rho_s - \rho_\infty)\,. \tag{2}$$

The linearized (or, more simply, linear) theory of evaporation and condensation from (into) semi-infinite space was developed by Labuntsov and Muratova [10] in 1969 as an extension of Labuntsov's study [11] of evaporation–condensation.

A one-dimensional stationary problem was considered, i.e., the general Boltzmann equation in the absence of mass forces,

$$\frac{\partial f}{\partial t} + \xi_x\frac{\partial f}{\partial x} + \xi_y\frac{\partial f}{\partial y} + \xi_z\frac{\partial f}{\partial z} = J\,,$$

where J is the collision integral

$$J = \int_0^\infty\int_0^{2\pi}\int\int_{-\infty}^{\infty}(f'f_1' - ff_1)|\mathbf{g}|b\,\mathrm{d}b\,\mathrm{d}\varepsilon\,\mathrm{d}\boldsymbol{\xi}_1\,,$$

took the form

$$\xi_x\frac{\partial f}{\partial x} = J\,.$$

We use here standard notations in the Boltzmann equation, as in [12].

The solution was found by the moments method based on discontinuous approximations of the molecular velocity distribution function. The choice of an approximation of specifically this type is due to the physical features characteristic of the evaporation–condensation process. Thus, from the very beginning, the most essential features of the process mechanism were incorporated in the approximation. To establish the degree of reliability of the solution, six- and eight-moment approximations were used in the analysis. The equation of the Bhatnagar–Gross–Krook model was solved along with the Boltzmann equation for Maxwellian molecules. Due to the inequalities

$$\frac{\rho_s - \rho_\infty}{\rho_s} \ll 1\,, \qquad \frac{T_s - T_\infty}{T_s} \ll 1\,,$$

the problems under study being only restricted by processes with relatively low nonequilibrium and, consequently, low transfer intensities, the nonlinear terms in the expressions for the moments of the distribution function and the collision integral in the system of equations that replaces the Boltzmann equation could be reduced to a linear form.

Such a simplification of the system of equations enabled derivation of the following equations for the relationship between the specific flows of mass, momentum, energy, and temperature jumps at the interface, and the differences between the corresponding pressures:

$$\tilde{j} = \frac{\beta}{1-0.4\beta}\,\frac{P_s - P_\infty}{2\sqrt{\pi}P_s} - \frac{\beta}{1-0.4\beta}\,\frac{0.44\tilde{q}}{2\sqrt{\pi}}\,, \tag{3}$$

$$\frac{T\big|_{x=0} - T_s}{T_s} = -0.45\,\tilde{j} - 1.05\tilde{q}\,, \tag{4}$$

$$\tilde{j} = \frac{j}{\rho_s\sqrt{2RT_s}}\,, \quad \tilde{q} = \frac{q}{P_s\sqrt{2RT_s}}\,, \quad \Delta\tilde{P} = \frac{P_\infty - P_s}{P_s}\,,$$

$$\tilde{j} \ll 1\,, \quad \tilde{q} \ll 1\,, \quad \Delta\tilde{P} \ll 1\,.$$

The solutions obtained were used to make conclusions about the specific state of the vapor near the interface. Namely, if the condensation coefficient is unity, the vapor is overheated during condensation and supersaturated during evaporation. The linear theory was further developed in studies [13–22] that confirmed the validity of Eqns (3) and (4) and their usefulness for practical applications.

2.2 Intense evaporation and condensation

2.2.1 Intense evaporation. S I Anisimov published in 1968 in the *Journal of Experimental and Theoretical Physics* an article [23] which initiated active studies of intense evaporation that occurs under laser irradiation and subsequent condensation. A theory of intense evaporation was developed shortly afterward in [24–29].

Intense evaporation is realized in a natural way in laser ablation. Review [30] notes that "the Russian thesaurus of the concepts of 'loss' and 'damage' includes the words 'evaporate' and 'escape', which are directly related to the ablation process." The same study showed in considering the thermal model of ablation (the near-surface evaporation model) that a stationary evaporation wave with calculable parameters may emerge, and it was argued that "the results of calculations based on the thermal model are in good agreement with the experimental data in the nanosecond range."

Studies on the theory of intense evaporation and condensation are also reported in [31–54]. An approximate

method was proposed in [34], the essence of which is as follows. The solution of the conservation equations for continuous media showed that a Euler inviscid flow is realized in the gas-dynamic region during evaporation. The velocity distribution function of molecules, which describes the state of vapor in this region, is consequently Maxwellian with a density ρ_∞, temperature T_∞, and macroscopic transfer velocity u_∞. Following the generally accepted diffusion scheme of evaporation with a condensation coefficient equal to unity, there are reasons to believe that the velocity DF of evaporated molecules is a half-Maxwellian with a known temperature of the interface.

Thus, the formulation of the problem sets the form of the distribution function of molecules far from the interface in the entire velocity space: it is the Maxwell distribution with the parameters ρ_∞, T_∞, and u_∞, one of which is known. The form of the DF of molecules moving from the interface towards the vapor and the quantities that characterize this DF near this surface are specified: it is half-Maxwellian with a temperature T_s and a density ρ_s that corresponds to the temperature T_s along the saturation line. The form of the DF of molecules moving to the interface from a vapor and the quantitative values that characterize the DF near this surface are unknown. We assume that the DF for these molecules is a half-Maxwellian with a temperature T_∞, a transfer rate u_∞, and an unknown density ρ_-. The assumption made makes it possible to reduce the problem of determining the mass flux density during evaporation $j = \rho_\infty u_\infty$ to solving a system of conservation equations represented in terms of the moments of the velocity distribution functions of vapor molecules near and far from the interface. Indeed, the conservation equations in the formulation under consideration are the conditions that flows of mass, momentum, and energy on the interphase plane at $x = 0$ and far from it, at $x \to \infty$, on the scale of the mean free path of vapor molecules be the same, where x is the normal coordinate in the vapor area. The listed flows may be represented in a known way as the moments of the corresponding DFs. The three conservation equations contain as a result six quantities: ρ_s, T_s, ρ_-, ρ_∞, T_∞, and u_∞, of which three, for example, ρ_s, T_s, ρ_∞, are considered to be specified. Consequently, this system of conservation equations is closed in the sense of determining the remaining unknown parameters $\rho_-, T_\infty, u_\infty$, and it can be successfully solved.

The results of the study of intense evaporation are as follows.

• Evaporation is a one-parameter problem, i.e., to determine the evaporation rate and all the quantities in the gas-dynamic region, it is sufficient to set only one quantity far from the Knudsen layer, for example, the vapor density ρ_∞ at a distance l large compared to the mean free path of vapor molecules.

• The vapor velocity during evaporation cannot be greater than the local sound velocity, i.e., the maximum value of the Mach number of the moving vapor is equal to one.

• The specific mass flux during evaporation for a one-dimensional stationary setup is 80–84% of the mass flux density of molecules evaporated from the interface, in accordance with the diffuse evaporation scheme.

• Density, temperature, and pressure during evaporation may significantly differ from the corresponding values for the interface determined based along the saturation line. For example, for the limiting mode of evaporation, the pressure in the gas-dynamic region P_∞ is only about 20% of the saturation pressure P_s determined from the interface temperature T_s.

• At high evaporation rates, the form of the DF of molecules that move to the interface near this surface has little effect on the value of the determined mass flux density.

• The vapor moving from the interface, which is formed as a result of evaporation, turns out to be highly supersaturated, which can lead to spontaneous homogeneous condensation of this vapor.

• To calculate the evaporation rate, the following formula is proposed, which approximates the calculations in [54] of the mass flux density during evaporation in the range where a one-dimensional stationary solution of this problem exists:

$$j_u = 0.6\sqrt{2RT_s}\,(\rho_s - \rho_\infty)\sqrt{\frac{\rho_\infty}{\rho_s}}. \tag{5}$$

2.2.2 Intense subsonic and supersonic condensation. It follows from the system of conservation equations for a continuous medium [54] that, during condensation in the gas-dynamic region, the Navier–Stokes flow is realized, in which the viscosity and thermal conductivity of the condensed flow manifest themselves. The solution of the conservation equations in the case of a one-dimensional stationary semi-infinite formulation may be represented then as a relationship between the velocities and temperatures of vapor at the outer boundary of the Knudsen layer and at $x \to \infty$.

Conjugation with the gas-dynamic region occurs in the macroscopic sense in a certain section, which we denote as K – K. It should be noted that such conjugation occurs on a kinetic scale in a thin layer (whose thickness is of the order of the mean free path of vapor molecules in the Knudsen layer). The velocity DF of vapor molecules in the Navier–Stokes region should not be Maxwellian, but a nonequilibrium one that takes into account the viscosity and thermal conductivity of the medium. The 13-moment approximation is known to have such properties; it leads in the one-dimensional formulation under consideration to a DF of the form

$$f_k = n_k\left(\frac{1}{2\pi RT_k}\right)^{3/2}\exp\left(-\frac{c^2}{2RT_k}\right) \times\left[1 - \frac{\tau_{xx}}{2P_k}\,\frac{c_x^2}{RT_k} - \frac{q_x}{P_k}\,\frac{c_x}{RT_k}\left(1 - \frac{1}{5}\,\frac{c^2}{RT_k}\right)\right], \tag{6}$$

where $P_k = \rho_k RT_k$, $n_k = \rho_k/m$, c_x is the projection of the relative velocity of the molecule on the x axis, $c_x = \xi_x - u_k$, τ_{xx} is the viscous stress tensor component, and q_x is the specific heat flux along the x axis.

When the molecules flying from the interface (condensation surface) pass through the Knudsen layer, if they collide with each other or with other molecules, the function f_k changes. Based on the same arguments as in the analysis of evaporation, we assume that the DF of incident molecules on the condensation surface is similar to the function presented above for $\xi_k < 0$, i.e., the DF in the immediate vicinity of the interface (cross section 0 – 0) has the form (6) in which the replacement $n_k \to Cn_k$ is made, where C is a certain parameter. If, at a known temperature of the interface T_s and therefore corresponding n_s, two of the three values P_∞, T_∞, u_∞ are set (in practice, P_∞, T_∞ are usually specified to determine u_∞), the number of unknown parameters is seven: u_∞, T_k, n_k, u_k, τ_{xx}/P_k, q_1/P_k, and C. To determine them, two

systems of equations of conservation of fluxes of mass, momentum, and energy are formulated: one for the cross sections $0-0$ and $K-K$, the other for $K-K$ and $\infty-\infty$, i.e., in total six equations. The expressions for the corresponding fluxes are written in terms of the parameters of the distribution functions at the coordinates $0-0$, $K-K$, and $\infty-\infty$. The seventh equation is obtained from the solution of the system of Navier–Stokes equations for the gas-dynamic region in the form of the dependence of u/u_∞ on x, written for $x = 0$ (on the gas-dynamic scale) in the form of the relationships among T_∞, u_∞, T_k, and n_k. This yields a closed system of equations, the solution of which determines all unknown parameters of the distribution functions and their moments: density, temperature, pressure, velocities, and mass, momentum, and energy fluxes.

Results of studies of intense condensation at subsonic speeds.

• The problem of subsonic condensation is two-parametric, i.e., to determine the mass flux density j during condensation (condensation rate), two of the three gas-dynamic quantities should be known outside the Knudsen layer, for example, the density $\rho_\infty(n_\infty)$ and the temperature T_∞. The third quantity, the velocity u_∞ or the Mach number M_∞, is determined as a result of the solution. Thus, the solutions for subsonic condensation can be represented as the dependence of n_∞ on T_∞ and M_∞ (or, possibly, the dependence of M_∞ on n_∞ and T_∞), i.e., as a surface in the $n_\infty, T_\infty, M_\infty$ space or sections of this surface for various values of M_∞ on the n_∞, T_∞ plane as in Fig. 1; here and below, $n' = n_\infty/n_s$, $T'_\infty = T_\infty/T_s$.

• Vapor density can both increase and decrease as vapor approaches the interface. The macroscopic velocity of the condensed vapor changes consequently in the opposite way. In this case, the vapor pressure remains in the first approximation nearly constant.

• The proposed method gives the results in the slow condensation area that virtually coincide with the predictions of the linear theory by Labuntsov and Muratova.

• Evaporation and condensation are nonsymmetric processes, primarily due to the nature of the flow of vapor in the gas-dynamic region. As the intensity decreases, this asymmetry decreases.

• To calculate the condensation rate (mass flux density), the following formula is proposed, which approximates the calculated density [54] of the mass flux during condensation in the range where a one-dimensional stationary solution of this problem at subsonic velocities of the condensing vapor flow exists:

$$j_k = 1.67\,\frac{P_\infty - P_s}{\sqrt{2\pi R T_\infty}}\left[1 + 0.51\,\ln\left(\frac{P_\infty}{P_s}\sqrt{\frac{T_s}{T_\infty}}\right)\right]. \qquad (7)$$

The calculation made using Eqn (7) is in good agreement with the results displayed in Fig. 1, which were obtained in [47] by solving the Boltzmann kinetic equation using the moment method.

The solution of the system of moment equations shows that a stationary shock wave may form at certain density and temperature near the interface. Figure 2 displays such a solution for the Mach number $M_\infty = 1.18$. If the pressure increases, a solution to the problem exists, but the nature of the dependences $n' = f_1(x)$ and $T' = f_2(x)$ changes.

In investigating the problem of a one-dimensional drain (an analogue of one-dimensional condensation), the CM methods were used to prove the uniqueness of the solution for a supersonic flow with a shock wave structure (see Appendix 2 of [55]). Reported there is also an analysis of the stability of possible solutions of the system of one-dimensional stationary conservation equations for any Mach number in the formulation under consideration. This analysis has shown that the system has a unique solution at subsonic velocities of vapor motion, while at supersonic velocities, the number of solutions is infinite large.

The analysis of the solutions for subsonic and supersonic condensation regimes shows that the results obtained using different methods of solving the kinetic equation for various potentials of interaction between molecules — hard elastic balls, Maxwellian and pseudo-Maxwellian molecules — are in the first approximation close to each other.

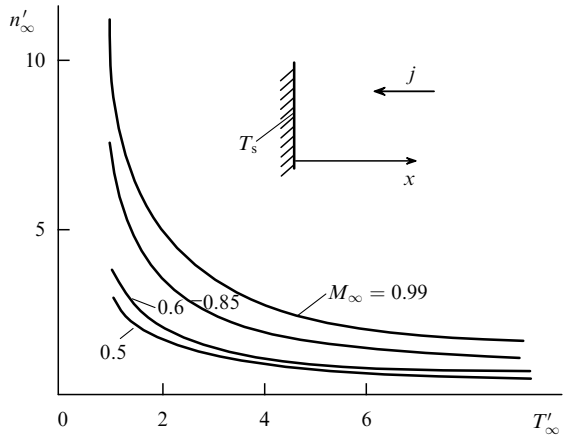

Figure 1. Solutions to the problem for determining the velocity of vapor in subsonic evaporation presented in terms of dimensionless density $n'_\infty = \rho_\infty/\rho_s$ as a function of dimensionless temperature $T'_\infty = T_\infty/T_s$ for various values of the Mach number M_∞ of the incoming flow of monatomic vapor. The displayed data enable finding for given n'_∞ and T'_∞ the unique value of M_∞ and, consequently, the velocity of the vapor.

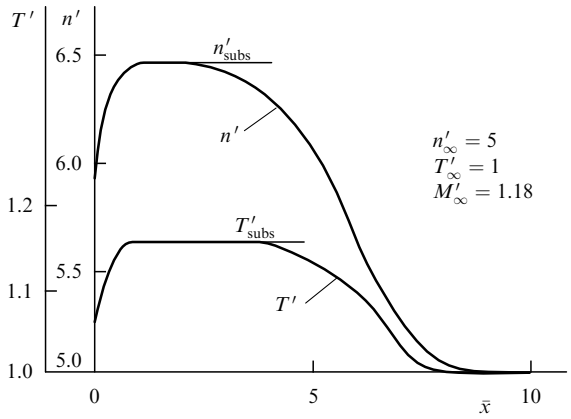

Figure 2. Changes in density and temperature in subsonic condensation in the limiting regime. The coordinate $\bar{x}$ is measured in free path units: $\bar{x} = x/l$, where l is the free path of vapor molecules calculated using the phase interface temperature T_s and the equilibrium numerical density of molecules n_s that corresponds to this temperature along the saturation line. The results obtained from the solution of the Boltzmann kinetic equation using the moment method show that a structure of a stationary shock wave (compression shock wave) is formed. The formation of a subsonic region with the dimensionless density n'_{subs} and T'_{subs} near the interphase surface is seen to occur.

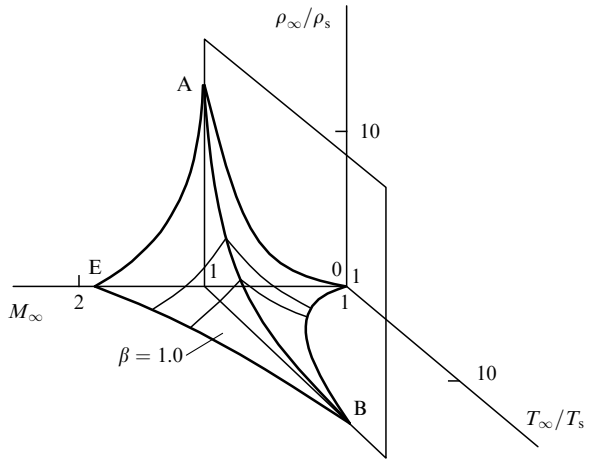

Figure 3. Solution to the problem of condensation displayed in a 3D space of dimensionless density $n'_\infty = \rho_\infty/\rho_s$, temperature $T'_\infty = T_\infty/T_s$, and Mach number M_∞ for condensation coefficient $\beta = 1$. The subsonic solutions are located on the surface of the curvilinear triangle A0B, and the supersonic solutions in the part of the space considered outer with respect to surface AEB. Solutions with the structure of a stationary shock wave similar to that displayed in Fig. 2 are located on the surface AEB.

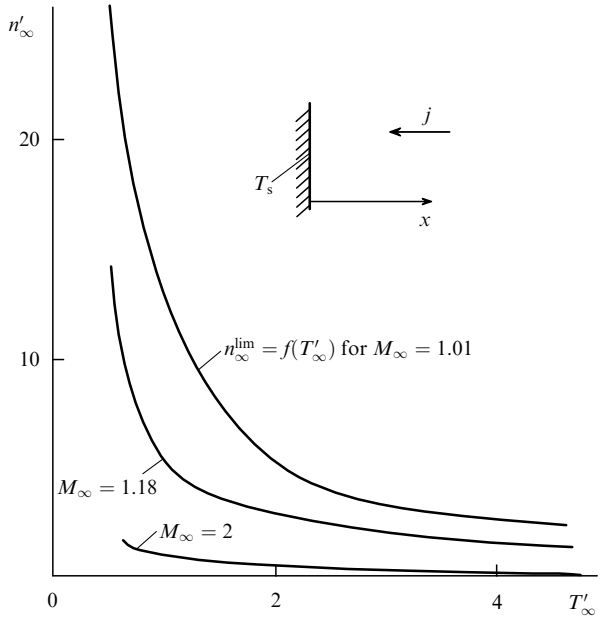

Figure 4. Sections of the surface AEB shown in Fig. 3 by the planes $M_\infty = \text{const}$. Displayed are limiting dependences of the dimensionless density n'_∞ on dimensionless temperature T'_∞ at which supersonic inflow of vapor with the structure of a stationary shock wave similar to those displayed in Fig. 2 occurs.

The results of the study of evaporation and condensation can be graphically depicted in three-dimensional space $n_\infty(\rho_\infty), T_\infty, M_\infty$, whose part corresponding to condensation is shown in Fig. 3 [47]. Thin lines in this figure are obtained as a result of cutting curvilinear figure A0BE by planes $T_\infty/T_s = \text{const}$, specifically $T_\infty/T_s = 3$ and $T_\infty/T_s = 5$. The sections of this figure divided by planes $M_\infty = \text{const}$ are shown in Figs 1 and 4. Solutions to the evaporation problem are displayed in the other half of the space with positive values of the Mach number M_∞.

We now list the main features characteristic of the presentation employed for the results of the study of evaporation–condensation problems in the $n_\infty, T_\infty, M_\infty$ space.

The equilibrium state is determined in this space by a single point with coordinates $n'_\infty = 1$, $T'_\infty = 1$, $M_\infty = 0$.

As noted above, to solve the problem of evaporation, it is necessary to set one of the gas-dynamic quantities away from the interface: n_∞ or T_∞, or $u_\infty(M_\infty)$. Evaporation is represented as a consequence as a line in the $n_\infty, T_\infty, M_\infty$ space.

The study of the problem of subsonic condensation carried out above shows that two quantities should be set to find its unique solution, for example, n_∞ and T_∞. Solutions are consequently located in the $n_\infty, T_\infty, M_\infty$ space on curvilinear triangle A0B shown in Fig. 3 and on this triangle alone due to the uniqueness of the solution at subsonic speeds.

It should be noted that the domain of application of the linear theory of evaporation–condensation is limited in $n_\infty, T_\infty, M_\infty$ space by a conventional sphere of small diameter centered at the origin.

For supersonic condensation (i.e., for $M_\infty > 1$), all three quantities are set: n_∞, T_∞, M_∞, implying that the solution to the problem becomes a three-parametric one. Any point in space to the left of the AEB surface represents in this case a feasible condensation regime with a supersonic vapor velocity. The points located directly on curvilinear triangle AEB represent the modes of supersonic condensation with the structure of the solution in the form of a stationary shock wave. Figure 3 shows that, as the Mach number M_∞ increases, the region where supersonic condensation exists expands. On the other hand, this figure shows a region of initial values exists for which stationary condensation, both subsonic and supersonic, cannot occur. This area is determined by the volume enclosed between the curvilinear triangle of subsonic condensation A0B and the surface of the limiting parameters of supersonic condensation AEB. Sections of the AEB surface by planes $M_\infty = \text{const}$ are shown in Fig. 4.

2.3 Effect of the condensation coefficient

2.3.1 Recalculation of the solution for the diffuse scheme of evaporation and reflection of molecules at arbitrary values of the evaporation–condensation coefficients. The relationships presented in Section 2.2 were derived for the case of complete condensation of molecules incident on the interface, i.e., a condensation coefficient equal to unity. We now derive, following [25, 44], expressions that enable the calculation of evaporation and condensation for arbitrary values of the evaporation β_e and condensation β_c coefficients for the diffuse scheme of reflection of noncondensed molecules. Due to this scheme of reflection, the DF of the molecules that move from the interface is a half-Maxwellian with the total density of evaporated and reflected molecules. Thus, the mass flux density of the molecules that move from the interface, j_+, is a sum of the mass flux densities of the evaporated, j_e, and the reflected, j_r, particles, i.e., $j_+ = j_e + j_r$.

At the same time $j_e = \beta_e n_s m\sqrt{RT_s/(2\pi)}$. Using the definition of the condensation coefficient $\beta_c = 1 - |j_r/j_-|$, where j_- is the density of the mass flux of molecules that move towards the interface, given that $j_r > 0$ and $j_- < 0$, we obtain $j_r = (\beta_c - 1)j_-$. Hence,

$$j_+ = \beta_e n_s m\sqrt{\frac{RT_s}{2\pi}} + (\beta_c - 1)j_- .$$

Since $j = j_+ + j_-$,

$$j_+ = \beta_e n_s m \sqrt{\frac{RT_s}{2\pi}} + (\beta_c - 1)(j - j_+)\,,$$

whence follows

$$j_+ = \frac{\beta_e}{\beta_c}\, n_s m \sqrt{\frac{RT_s}{2\pi}} + \frac{\beta_c - 1}{\beta_c}\, j\,.$$

If the last formula is presented as $j_+ = \rho_0 \sqrt{RT_s/(2\pi)}$, we find that the vapor density at the interface is

$$\rho_0 = \rho_s \left(\frac{\beta_e}{\beta_c} - \frac{1 - \beta_c}{\beta_c}\, \frac{j}{\rho_s \sqrt{RT_s/(2\pi)}} \right).$$

Based on Eqns (5) and (7), an algorithm can be proposed to calculate the mass flux density during intensive evaporation and condensation for arbitrary values of the condensation and evaporation coefficients. The essence of the algorithm for subsonic velocities is eventually that a single calculation relation — Eqn (5) for evaporation or Eqn (7) for condensation — is now replaced by a system of two equations for evaporation, which contain two unknown quantities j and ρ_0, and a system of three equations for three unknowns j, ρ_0, and P_0, for condensation. The system for evaporation is

$$\begin{aligned} j &= 0.6\sqrt{2RT_s}\,(\rho_0 - \rho_\infty)\sqrt{\frac{\rho_\infty}{\rho_s}}\,, \\ \rho_0 &= \rho_s \left(\frac{\beta_e}{\beta_c} - \frac{1 - \beta_c}{\beta_c}\, \frac{j}{\rho_s \sqrt{RT_s/(2\pi)}} \right), \end{aligned} \tag{8}$$

while the system for condensation is

$$\begin{aligned} |j| &= 1.67\, \frac{P_\infty - P_0}{\sqrt{2\pi RT_\infty}} \left[1 + 0.51 \ln \left(\frac{P_\infty}{P_0} \sqrt{\frac{T_s}{T_\infty}} \right) \right], \\ \rho_0 &= \rho_s \left(\frac{\beta_e}{\beta_c} + \frac{1 - \beta_c}{\beta_c}\, \frac{|j|}{\rho_s \sqrt{RT_s/(2\pi)}} \right), \\ P_0 &= \rho_0 R T_0\,. \end{aligned} \tag{9}$$

2.3.2 Limiting values of condensation coefficients and specific mass fluxes [44]. We now consider in more detail intense condensation. Equation (9) at $\beta_e = \beta_c = \beta$, given that $|j| = \rho_\infty|_{\beta \neq 1} |u_\infty|$, may be represented in the form

$$\rho_0 = \rho_s \left[1 + \frac{1 - \beta}{\beta}\, \frac{\rho_\infty|_{\beta \neq 1} |u_\infty|}{\rho_s \sqrt{RT_s/(2\pi)}} \right]. \tag{10}$$

If the condensation coefficient is other than unity, the role of ρ_s is played by ρ_0; therefore, the relation

$$\frac{\rho_\infty|_{\beta \neq 1}}{\rho_0} = \frac{\rho_\infty|_{\beta = 1}}{\rho_s} \tag{11}$$

holds valid. Taking ρ_0 from Eqn (11) and substituting it into Eqn (10), we obtain from the latter equation

$$\rho_\infty|_{\beta \neq 1} = \frac{\rho_\infty|_{\beta = 1}}{1 - \left[(1 - \beta)/\beta\right] (\rho_\infty|_{\beta = 1}/\rho_s) |u_\infty| / \sqrt{RT_s/(2\pi)}}\,. \tag{12}$$

This formula determines the minimum value of the condensation coefficient at which condensation with a given rate u_∞ is at all possible. The denominator in Eqn (12) vanishes at this value, i.e., $\rho_\infty|_{\beta \neq 1}$ tends to infinity. As a result, from Eqn (12), we obtain

$$\beta_{\lim} = \frac{1}{1 + 1/j'}\,, \tag{13}$$

where $j' = |j|_{\beta = 1}| / [\rho_s \sqrt{RT_s/(2\pi)}\,]$.

Intense condensation with given u_∞ and T_∞ occurs, for example, if cryogenic pumps are used in simulators of gas flow around various bodies, when the Mach number and temperature are set at the inlet. It is of use sometimes to represent formula (13) in terms of the Mach number. For example, for a monatomic gas, where the speed of sound a_∞ is calculated using the formula $a_\infty = \sqrt{(5/3)RT_\infty}$, we get

$$\beta_{\lim} = \left[1 + \sqrt{\frac{3}{10\pi}}\, \frac{1}{(\rho_\infty|_{\beta = 1}/\rho_s) |M_\infty| \sqrt{T_\infty/T_s}} \right]^{-1}. \tag{14}$$

Equation (14) may be used to find the dependence of $\beta_{\lim}$ on temperature. Figure 5a shows such a dependence for $M_\infty \to 1$, while Fig. 5b does so for $M_\infty = 2$. As can be seen in Fig. 5a, if $M_\infty \to 1$ and $T_\infty/T_s = 1$, supersonic condensation modes only exist at values of the condensation coefficient that lie in a narrow range from 1.00 to ≈ 0.96, and for $M_\infty = 2$ and $T_\infty/T_s = 1$, in a range from 1.00 to ≈ 0.85. If the condensation coefficient becomes less than these values, the supersonic flows in the one-dimensional stationary setup under consideration may not exist. In a real situation, a shock wave with the structure displayed in Fig. 2 emerges near the interface, which moves towards the incoming flow. Such a breakdown of this condensation regime can be explained by the fact that the mass flux density of the incoming vapor flow is high at high (supersonic) velocities, and should only a small fraction of this flow be reflected from the phase interface, it is sufficient for the reflected flow to become comparable to the evaporating flow. A significant increase in the vapor mass flow moving from the interface surface, which consists of evaporated and reflected flows, may be interpreted as a kind of increase in the temperature of this surface, which causes a sharp decrease in the condensation rate. In addition to the curves $\beta_{\lim} = f(T'_\infty)$ displayed in Fig. 5, the above relations enable derivation of the limiting pressure $P_{\lim}$, at which supersonic condensation with a given Mach number and temperature can occur, as a function of the condensation coefficient β. Such functions are shown in Fig. 6, and the corresponding data are presented in Table 1, where $P_{\beta=1}$ is taken from [47] and Fig. 4 as $P_{\beta=1} = n'_\infty T'_\infty$, while $P_{\beta_{\lim}} = (\rho_\infty|_{\beta \neq 1}/\rho_s) T_\infty$, $\rho_\infty|_{\beta \neq 1}$ is determined using Eqn (12).

The form of results obtained in studying evaporation–condensation in the $n_\infty, T_\infty, M_\infty$ space at condensation coefficient β different from unity is altered. For example, at $\beta = 0.96$, the results displayed in Fig. 3 take the form shown

Table 1. Limiting values of pressure $P_{\lim}$ for $\beta = 1$ and close to the limiting $\beta_{\lim}$, i.e., at $\beta = \beta_{\lim} + 0.004$.

M_∞	T_∞/T_s	$\beta_{\lim}$	$P_{\lim}\|_{\beta=1}$	$P_{\lim}\|_{\beta \to \beta_{\lim}}$	$P\|_{\beta_{\lim}}/P\|_{\beta=1}$
1.2	1.0	0.951	5.00	58.5	11.7
1.2	4.2	0.909	5.31	160.0	30.1
1.5	1.0	0.906	2.00	52.5	26.3
2.0	0.5	0.886	0.85	23.3	27.4
2.0	1.0	0.847	0.85	32.9	38.7
2.0	4.2	0.779	1.10	9.5	8.6
3.6	4.0	0.602	0.26	8.5	32.8

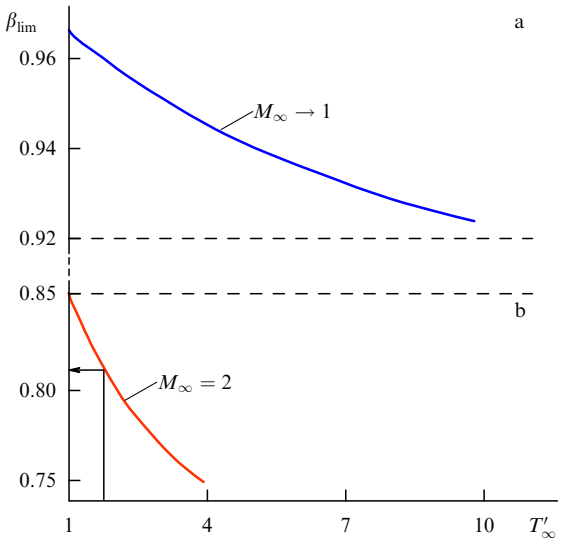

Figure 5. Temperature dependence of the limiting values of the condensation coefficient at which the regimes of supersonic stationary inflow are possible. (a) If $M_\infty \to 1$, even a small decrease in the condensation coefficient β results in the breakdown of condensation. As the Mach number increases, the range of the 'allowable' values of the condensation coefficient expands. (b) For $M_\infty = 2.0$ and values of the coefficient β in a range from 1.0 to 0.85, supersonic condensation may occur at $T'_\infty \geqslant 1$.

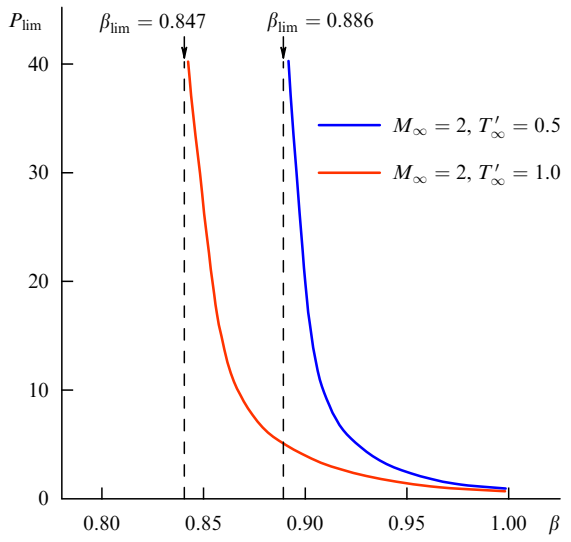

Figure 6. (Color online.) Limiting pressure for the occurrence of stationary supersonic condensation P_{lim} as a function of the condensation coefficient β. As β approaches the value β_{lim}, the limiting pressure increases and tends to infinity. For example, for $M_\infty = 2.0$ and $T'_\infty = 1.0$, such growth occurs when the condensation coefficient tends to $\beta_{\text{lim}} = 0.847$ (red curve).

in Fig. 7. It can be seen that even a small decrease in the condensation coefficient (by only 0.04) results in a noticeable transformation of the limiting 'supersonic' surface AEB and its shift to the left. Such a transformation describes the situation when the pressure P_∞ (or density ρ_∞) needed to ensure at a given value of T_∞ the required value of the Mach number M_∞ significantly increases, and the region of unacceptable parameters, i.e., such a combination of pressure, temperature, and incoming flow velocity for which the regime of supersonic condensation with constants T_∞ and M_∞ becomes not possible, expands. Figure 7 shows that the

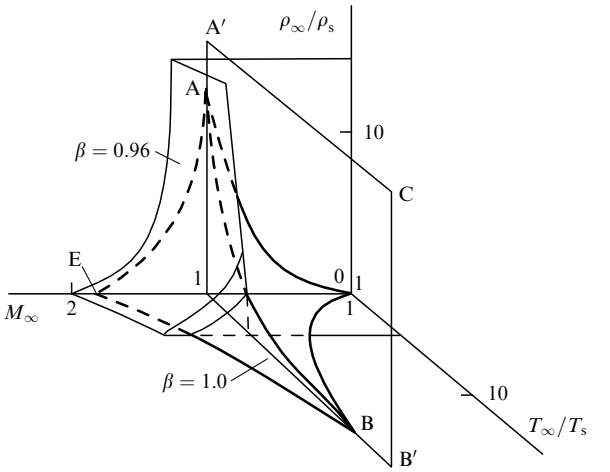

Figure 7. Solutions to the problem of condensation displayed in the three-dimensional space of dimensionless density, temperature, and velocity (Mach number) for the condensation coefficient $\beta = 0.96$. A similar plot for the condensation coefficient $\beta = 1.0$ is displayed for comparison. The comparison shows that a small decrease in the condensation coefficient near $M_\infty = 1.0$ for the given value of $T'_\infty = T_\infty/T_s$ results in a strong increase in $n'_\infty = \rho_\infty/\rho_s$.

decrease in β noted above results in a kind of opening of the depicted curvilinear pyramid.

3. Analysis of experimental data. Comparison with calculations

This section contains a systematic analysis of experimental studies of subsonic condensation of mercury and potassium vapors [56–59], intense evaporation of iodine [60, 61], supersonic cryogenic condensation of gas jets of nitrogen, argon [62–64], and air [65], and transfer processes on the interface of superfluid helium [66–74].

3.1 Intense condensation of metal vapors

The experimental setup designed to study the condensation of mercury vapor [56] was a closed circuit made of steel pipes, which included a boiler, an experimental segment, and an auxiliary condenser. Mercury vapor, moving downward, flowed onto the vertical plane of the test condenser, which was cooled with water or air. The auxiliary condenser located below the test condenser could be used to ensure the movement of vapor near the condensation surface to prevent the accumulation of noncondensable gases. Condensate from both condensers returned to the boiler as a result of draining. To observe the test condenser, the experimental setup had a window equipped with a heater to prevent condensation on it.

Temperature was measured using thermocouples. Holes for the thermocouples in the condensing unit were located parallel to the condensation surface in the central horizontal plane of the condensing unit. The thermocouple wires were output along isotherms. Two condensing blocks of the same size were used (the condensation surface was a square with a side of 40 mm).

The experimental procedure was as follows. First, the setup was prepared, namely, the circuit and its constituent elements were evacuated at a temperature of 540 K to a pressure of 10^{-2} Pa for several days, as a result of which gas was removed from the materials of the experimental setup. As noted in [56], it takes about 40 h to ensure complete wetting of the surface of the nickel coating of a copper condenser. In the

study under consideration, the components of the setup were kept prior to the experiment at a temperature of about 420 K for 7 h a day for six days.

The vapor temperature under steady-state stationary conditions was measured using two thermocouples. As follows from the analysis, the thermocouple readings are closer to the true temperature value at low vapor velocities and for the cross sections located near the region where the flow around the condensing block ends.

The surface temperature was determined in all the experiments by linear extrapolation of the temperature readings of the condensing unit as a function of the coordinate. The specific heat flux was consequently determined applying the Fourier law of thermal conductivity. The value of the heat flux was found by means of an alternative technique from the heat balance using the known flow rate of the coolant and the increase in its temperature as a result of pumping through the condensing unit. The results of these methods are in good agreement with each other. The accuracy of determining the surface temperature was about 0.1 K.

The difference between the readings of the thermocouples that measured the vapor temperature did not exceed 0.2 K at the maximum temperature. This difference at minimum temperatures was 0.6 K if the auxiliary condenser was not used, and about 1.2 K with it.

An analysis of the experimental techniques [56] and the estimated uncertainty of the measurements performed allow an assertion that the condenser surface temperature (accuracy 0.1 K) and the heat flux during condensation were determined in this study with high accuracy. The vapor parameters, the vapor temperature T_v of the vapor and its pressure P_v, were found with less accuracy. The difficulties related to measuring temperature in a moving flow are well known. Moreover, these flows were realized in the considered experiment at reduced pressures (50–5000 Pa), and the working substance was mercury.

The experimental results in the form of the temperature drop $\Delta T = T_v - T_s$ as a function of the mass flux density j are shown in Figs 8 and 9 with dots and triangles for two series of experiments, respectively. The general conclusions made by the authors of Ref. [56] during the initial analysis of the data obtained in the experiment are as follows: (1) the results for two condensing blocks are in good agreement with each other; (2) points for a given vapor temperature are located along a smooth continuous curve; (3) the sought-after relationship significantly depends on the vapor temperature.

To calculate the parameters of vapor with consideration for its expansion and acceleration as the condenser is approached, a system of equations for the conservation of mass, momentum, and energy was formulated in [55] for the conjugated problem of evaporation in a boiler, movement of the produced vapor along the working channel, and condensation. The rates of evaporation and condensation were determined in this case using Eqns (5) and (7). The solutions found are shown in Figs 8 and 9 with solid lines.

An analysis of the experimental data presented in [56] shows that, for condensation regimes characterized by high velocities of vapor movement, the effects of vapor compressibility and a decrease in temperature as a result of its expansion as the vapor approaches the condenser are significant. If the pressure of the condensed vapor P significantly differs from the pressure P_s along the saturation line, which corresponds to the temperature of the interphase surface T_s, the condensation rate is determined by the efficiency of

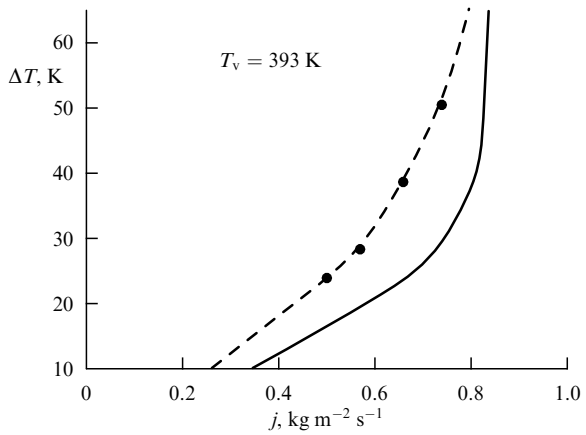

Figure 8. Results of experiments [56] on intense condensation of mercury at large velocities of the motion of vapor that are implemented at relatively low temperatures and pressure. j is the mass flux density, T_v is the temperature of condensed vapor, and $\Delta T = T_v - T_s$, where T_s is the temperature of the condensation surface. The nonlinear behavior of j as a function of ΔT obtained at large values of the difference between T_v and T_s indicates that the condensation rate is not limited in this case by the kinetic conditions at the phase interface but is determined by the gas-dynamic efficiency of the supply of mass to the interface. In other words, the surface adsorbs the entire mass delivered to it.

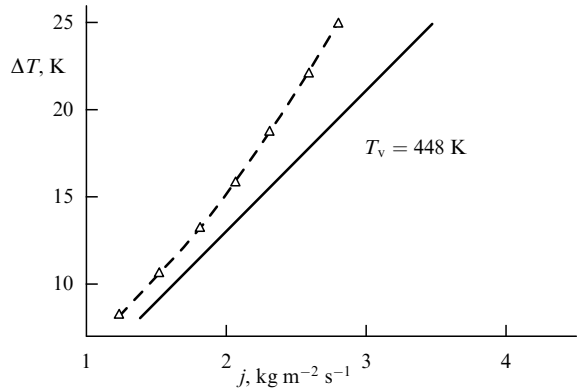

Figure 9. Results of experiments [56] on intense condensation of mercury at large mass flux densities. The velocities of the vapor flow in this case are not large, since pressure is significantly higher than in the flows displayed in Fig. 8, and the condensation rate is primarily determined by the kinetic conditions at the interface.

supplying the condensed vapor to the interface. Indeed, for the maximum vapor velocity obtained in [56], the ratio $P/P_s = 24$ at $T_v/T_s = 0.9$. It was noted in Section 2.2.2 that a supersonic condensation regime is realized for such a temperature ratio at $P/P_s > 15$. The condensation rate under these conditions can take on values larger than the mass flux determined for the conditions of formation of a shock wave near the condensation surface with the corresponding Mach number close to unity. Consequently, the condensation rate is not limited in this case by the kinetic conditions at the interface, but rather is determined by the efficiency of mass supply to this interface. In other words, the surface adsorbs all the mass that comes to it, i.e., the driving factor is the external flow of vapor that supplies the condensed vapor to the interface. According to the experimental data presented, these conclusions primarily pertain to modes with minimum temperatures of the interface and

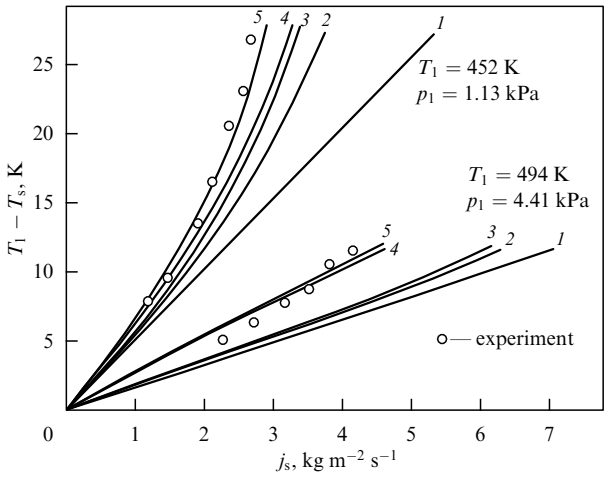

Figure 10. Results of experiments [58] on intense condensation of mercury and their interpretation. The result obtained in the minimal approximation (see Figs 8 and 9) (curve *1*) in comparison with the results obtained additionally taking into account the presence of broadening and narrowing segments of the vapor path (curve *2*), friction of the vapor against the channel walls (curve *3*), thermal resistance of the condensate film (curve *4*), and possible homogeneous condensation that occurs if the vapor expands (curve *5*), and with experimental results (circles).

condensable vapor, since its density is in this case low, and, therefore, the velocity of motion is significant.

The description of experimental data on intense condensation of potassium vapor presented in [57], which is based on the considered method, confirmed the validity and effectiveness of the above approach.

Later experimental data on mercury condensation [58] were interpreted in report [59] as a development of the above approach The corresponding results are displayed in Fig. 10. The following factors and parameters ignored in the minimal approximation considered above (line *1* in Fig. 10) were additionally taken into account in this case: the presence of expanding and narrowing sections of the vapor path (line *2*), friction of vapor against channel walls (line *3*), thermal resistance of the condensate film (line *4*), and the possibility of homogeneous condensation that occurs during the expansion of vapor (line *5*).

3.2 Intense evaporation of iodine

Intense evaporation of iodine was experimentally investigated in [60]. The longitudinal, $T_{\parallel}$, and transverse, $T_{\perp}$, temperatures, the transfer rate of vapor u, and its density ρ in the Knudsen layer were measured in [60] without introducing diagnostic techniques into this layer, namely, via fluorescence spectroscopy methods using a tunable laser. The absorption efficiency was determined from the intensity of the fluorescent light emitted by the excited (absorbed) molecules. The laser was tuned to record the full profile of one or more absorption bands of iodine molecules. Each band featured a highly pronounced structure consisting of many lines that overlapped due to Doppler broadening. The area of the absorption band is a measure of the density, and the bandwidth is a measure of the transfer rate.

The results of experiments are presented in report [60] for the interface temperature $T_s = 253$ K and $M_\infty = 0.66$ in the form of dependences $T_{\parallel}$, $T_{\perp}$, the Mach number, ρ, and the mass flux density j on the coordinate x normal to the interface surface. The experimental data were compared with the solution to the problem of intense evaporation obtained by the authors of [60] based on a five-moment approximation of the distribution function in the form of a two-flow Maxwellian with unknown ρ_1, T_1, ρ_2, T_2, and u. Index 1 refers to the molecules that move from the interface, and index 2 to those that move in the opposite direction. The moments of the collision integral were calculated in this case for Maxwellian molecules.

A comparison of the experimental and calculated data shows good agreement between the theory and experiment in the entire region, with the exception of a small mismatch near the phase interface. This circumstance requires, according to the authors of Ref. [60], a more thorough analysis of the boundary conditions at $x = 0$. It is also noted that the calculations based on the five-moment discontinuous approximation yield a greater thickness of the Knudsen layer and better agreement with experiment than the solutions previously obtained by the authors of [61] using an ellipsoidal DF. This situation seems to be quite natural, since the ellipsoidal continuous DF describes the molecules that move from the interface at $x = 0$ in a less accurate way than the two-sided discontinuous approximation.

3.3 Cryocondensation of nitrogen, argon, and air

A study of supersonic cryocondensation of gas jets of nitrogen and argon is presented in [62]. The experimental setup described in detail in Ref. [63], which is shown in Fig. 11, enabled the condensation of low-density gas jets to be explored. The vacuum chamber, which is a cylinder 200 mm in diameter, was completely immersed in liquid helium, so the temperature of its walls during the experiment was 4.2 K.

The efficiency of condensation was estimated based on the measurements made using a microbalance of the incident flow and the flow reflected from the cryopanel. It was found that an increase in the mass flow rate through the gas source leads to an increase in the mass flux density j and the velocity of the condensing flow. When complete condensation fails, a pressure wave is formed near the cryopanel, which begins moving towards the gas source if the temperature of the condensation surface rises. The flux reflected from the

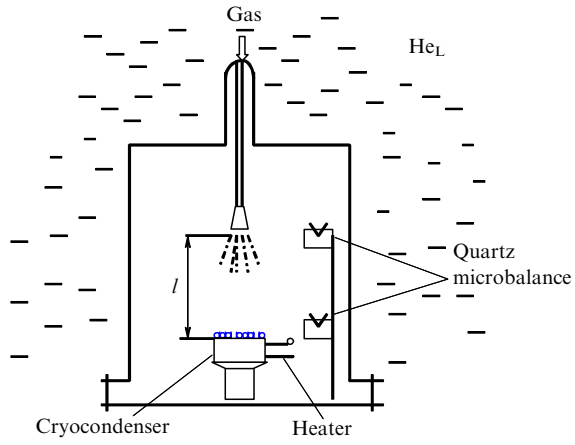

Figure 11. Experimental setup for studying supersonic cryocondensation of gas jets of nitrogen and argon input through various detachable sources (nozzles and diaphragms) located in the upper part of the working chamber. Gas jets are desublimated on a cryocondenser located on the lower flange. Reflected and direct flows are detected by a quartz microbalance whose sensitive elements are oriented towards the incoming flow.

cryopanel cannot be measured in this case using a quartz microbalance, but the formation and passage of a pressure wave can be recorded. The purpose of this experiment was to determine the temperature of the condensation surface at which the pressure wave emerges at the cryopanel, i.e., the complete condensation of the supersonic gas flow fails, as a function of various parameters (velocity, density, etc.). The studies were carried out for three gases: argon, nitrogen, and carbon dioxide.

In the case of a free-molecular flow of a condensed gas, the flow parameters are considered constant on the entire path from the gas source to the cryopanel, and the condensation rate is determined by the effective condensation coefficient. The following gas sources were used to investigate in the free-molecular mode: (1) a diffuser 8 mm in diameter, made of several layers of a wire gauze with 64-μm cells, that enables production of a gas flow uniformly distributed in all directions; (2) a 4-mm diaphragm; (3) a Laval nozzle with a critical section diameter $d_* = 0.98$ mm and a half opening angle $\theta_a = 12°$. For sources of all three types, the condensation surface temperature T, at which the flow reflected from the cryopanel is detected, as a function of the specific mass flow j entering the cooled surface was obtained. At high mass flux rates, the diaphragm and various nozzles were used as gas sources.

Figure 12 shows the dependence $j = f(T)$ for argon at high values of the mass flux density. The distance from the gas source to the cryosurface varied from 27 mm to 45 mm; one nozzle had a throat diameter of $d_* = 1.5$ mm and a half-opening angle of $\theta_a = 15°$, the other had $d_* = 0.98$ mm and $\theta_a = 15°$; the gas temperature in the settling chamber (slowdown temperature) in the first case was 100 K, and in the second 300 K. It can be seen that a higher temperature of the termination of full condensation corresponds to the regions of continuous flow of greater length that are formed at lower values of θ_a and d_* for a fixed flow rate after gas outflow from the source. This phenomenon is due to the fact that an increase in the continuous flow region leads to a corresponding change in the parameters of the gas flow (temperature, velocity, and density).

The conducted experimental study allowed drawing the following conclusions:

• for $j \leqslant 10^{-3}$ kg m^{-2} s^{-1}, the efficiency of condensation only depends on the specific mass flow onto the cryopanel and its temperature T;

• an increase in the gas flow rate to larger values results in the formation of a continuous flow zone at the outlet of the gas source and, hence, in a change in the condensed flow parameters. The flow velocity significantly exceeds in this case that of sound, while the condensation efficiency is determined by the geometry and type of gas source, the distance from the source to the cryopanel, and the slowdown temperature.

The presented conclusions are confirmed by the calculations of supersonic condensation based on solving the Boltzmann kinetic equation. An example of a solution to a two-dimensional problem of gas outflow from a nozzle into vacuum and condensation of the forming flow on a cryopanel is given in [64], where a flow was explored, which is characterized by the Knudsen number Kn = 0.33 at the exit of the slot-like nozzle and the Mach number $M = 2$. The Kn number was determined from the nozzle height, and M from the longitudinal velocity and temperature at the nozzle outlet. The solutions were found for various temperatures of the condensation surface.

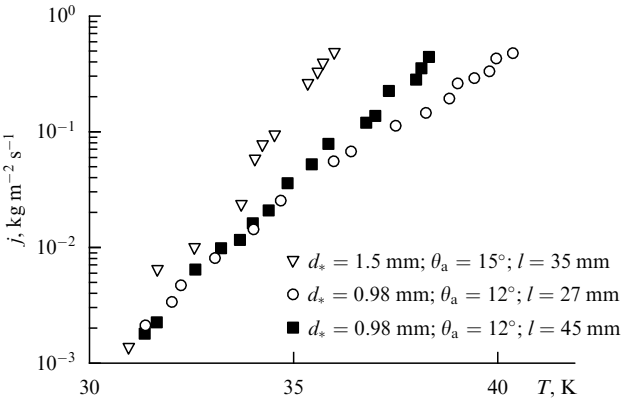

Figure 12. Experimental data on cryocondensation of supersonic argon jets. T is the temperature of the condenser surface, l is the distance from the source to the surface of the condenser, j is the density of the mass flux of the gas being desublimated (condensation rate). Used as gas sources were a Laval nozzle with a critical section diameter $d_* = 1.5$ mm and a half-opening angle $\theta_a = 15°$ and a Laval nozzle with $d_* = 0.98$ mm and $\theta_a = 12°$. For the given values of the condensation rate, the highest temperatures of the interface were obtained at which complete condensation occurs, i.e., the entire $T-j$ quadrant is divided into two subregions: complete condensation is possible to the left of the experimental points, and not possible to the right. For example, for the Laval nozzle with $d_* = 1.5$ mm and $\theta_a = 15°$ located at a distance of 35 mm from the condenser, desublimation is complete at $j = 0.01$ kg m^{-2} s^{-1}, i.e., there is no reflected flow if the interface temperature does not exceed 32.5 K.

In the experiment described in report [65], air (a mixture of 78% nitrogen, 21% oxygen, and 1% argon) flowed at the Mach number $M_\infty = 2.8$ and temperature $T_\infty = 186$ K onto a cryopanel cooled with liquid helium. The flow time was 18–25 s, and the temperature of the condensation surface increased from 4.2 K to 34–38 K. If the cryocondenser was cooled with liquid neon, the corresponding values were 9 s and 38.2 K. A pressure wave was formed near the cryosurface when its temperature was about 38 K, which was visually recorded. In the first approximation, we take the cryopanel temperature to be equal to the condensation surface temperature T_s. The pressure in the air flow P_∞ was 0.73 Pa, and the ratio of the flow temperature $T_\infty = 186$ K and the temperature of the interface T_s was $186/38 = 4.9$. In accordance with Refs [45, 47], for such a ratio T_∞/T_s and $M_\infty = 2.8$, a pressure wave emerges at the interface at $P_\infty/P_s = 0.46$, where P_s is the saturation pressure that corresponds to temperature T_s, i.e., $P_\infty = 0.46P_s$. Consequently, $P_s = 1.59$ Pa for the experimentally determined pressure $P_\infty = 0.73$ Pa. According to the empirical dependence for nitrogen [75], $P_s = 10^{-385.0/T_s+10.3}$, this pressure corresponds to $T_s = 38.0$ K, a value which is in good agreement with the experimental data (34–38 K and 38 K (see above)). Similar calculations made for various values of the condensation coefficient β show that agreement with experiment is best at $\beta \approx 1$. Thus, it may be concluded that the condensation coefficient during cryocondensation of a supersonic air flow with a Mach number of 2.8 is close to unity.

3.4 Interpretation of experimental data on transfer processes at the helium II interface

3.4.1 Evaporation of superfluid helium due to heat supply to the phase interface from the liquid. Experiments were carried out in the late 20th century to study the evaporation of helium II (He II) [66, 67]. It is generally believed that studies of the

evaporation and condensation of specifically helium II may provide the most promising information on transfer processes on interphase surfaces for the following reasons. First, both the vapor and the liquid are free of impurities and noncondensable components, since all other substances at such low temperatures (< 2.17 K) simply freeze (turn into a solid). Second, the efficiency of heat transfer in He II is maximal among all materials. Consequently, the effects on the interface are barely masked by the thermal resistance of the liquid, i.e., it turns out that phenomena at the interface may be explored in the clearest way possible.

An experimental cell [66] was immersed in He II maintained in a cryostat with optical windows, which made it possible to visualize the motion of the vapor and the change in its density during evaporation; a holographic laser interferometer was used to this end. A heater in the form of a thin nichrome film was placed at the bottom of the vessel with He II. The heat produced by the heater propagated from bottom to top through the helium II by the second-sound wave and reached the liquid–vapor interface, on which evaporation occurred. A density perturbation emerged in this case in the vapor, which propagated from the interface. The motion of this perturbation was recorded by an interferometer. A superconducting thermometer, a pressure sensor, and a hot-wire flow meter were used to measure the temperature, pressure, and vapor velocity, respectively.

The authors of [66] determined as a result of experiments the temperature T_s (in the notation of this review) of the liquid (He II)–vapor interface, and, consequently, the pressure along the saturation line P_s, the vapor pressure during evaporation P_∞, and the velocity of its motion V_∞. Experimental data were presented in the form of dependences P_∞/P_s on $V_\infty/\sqrt{2RT_s}$ similar to those shown in Fig. 13 for various initial temperatures of superfluid helium T_1.

The following interpretation of these results has been proposed [68]. First, unlike the authors of most studies in this area, we assume that the evaporation coefficient β_e is not equal to the condensation coefficient β_c. The formulas of the linear theory of Labuntsov and Muratova (see Section 2.1) can be generalized for this case. It is sufficient to this end to rederive the Kucherov–Rikenglaz formula for $\beta_e \neq \beta_c$. We obtain as a result an equation that determines the mass flux density j for weak evaporation–condensation:

$$j = \frac{1}{1-0.4\beta_c}\sqrt{\frac{RT_s}{2\pi}}\,(\beta_e\rho_s - \beta_c\rho_\infty)\,, \tag{15}$$

instead of $j = \beta/(1-0.4\beta)\sqrt{RT_s/(2\pi)}\,(\rho_s - \rho_\infty)$ for $\beta_e = \beta_c$.

The same transformations yield the following form of the Labuntsov–Muratova formula for evaporation into a semiinfinite space for $\beta_e \neq \beta_c$:

$$j = \frac{1}{1-0.4\beta_c}\sqrt{\frac{RT_s}{2\pi}}\,(\beta_e\rho_s - \beta_c\rho_\infty) = \frac{1}{1-0.4\beta_c}\,\frac{\beta_e P_s - \beta_c P_\infty}{\sqrt{2\pi RT_s}}\,. \tag{16}$$

Applying the obtained relations to the experimental data displayed in Fig. 13 yielded the results presented in Table 2.

An analysis of the data displayed in Table 2 shows that the coefficients β_e and β_c are close to each other and to unity. It should be stressed at the same time that they are only close rather than exactly equal to each other. However, the equality

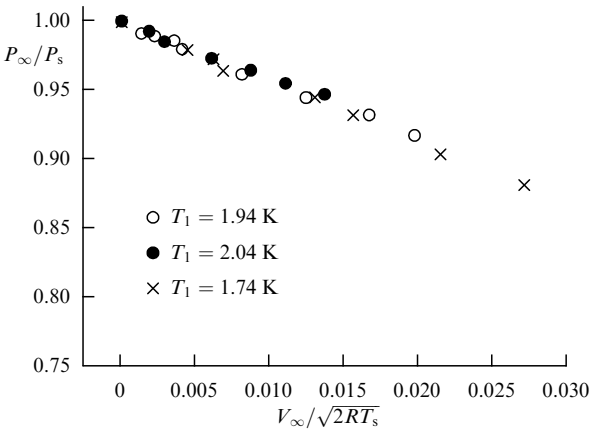

Figure 13. Results of experiments [66] on evaporation of superfluid helium due to impingement of a wave of the second sound from the liquid to the interface. The authors used the experimental data to determine the temperature T_s of the liquid (He II)–vapor interface and, hence, the pressure along the saturation line P_s that corresponds to this temperature, the vapor pressure of evaporation P_∞, and the velocity of motion V_∞. Experimental data are presented as dependences P_∞/P_s on $V_\infty/\sqrt{2RT_s}$ for various initial temperatures of superfluid helium.

Table 2. Results of calculations at various values of the evaporation and condensation coefficients.

$V_\infty/\sqrt{2RT_\infty}$	0.005	0.010	0.015	0.020
P_∞/P_s	0.97	0.95	0.93	0.91
β_c for $\beta_e = 0.95$	0.97	0.98	0.99	1.00
β_c for $\beta_e = 0.90$	0.92	0.92	0.93	0.94
$\beta_e = \beta_c = \beta$	0.48	0.55	0.58	0.60

leads to a significant difference from unity. Such a strong effect is due to a basically different form of calculation ratios. Namely, for $\beta_e = \beta_c = \beta$,

$$\frac{P_\infty}{P_s} = 1 - \frac{1-0.4\beta}{\beta}\,\frac{2\sqrt{\pi}\,V_\infty}{\sqrt{2RT_\infty}}\,,$$

$$\beta = \frac{V_\infty 2\sqrt{\pi}/\sqrt{2RT_\infty}}{0.4\,V_\infty 2\sqrt{\pi}/\sqrt{2RT_\infty} + 1 - P_\infty/P_s}\,,$$

and for $\beta_e \neq \beta_c$,

$$\beta_c = \frac{\beta_e - V_\infty 2\sqrt{\pi}/\sqrt{2RT_\infty}}{P_\infty/P_s - 0.4\,V_\infty 2\sqrt{\pi}/\sqrt{2RT_\infty}}\,. \tag{17}$$

Moreover, the calculation of the measurement errors carried out in [68] shows that, for example, given the same initial data, the error in determining β_c under the assumption $\beta_e = \beta_c$ is approximately twice as large as for $\beta_e \neq \beta_c$. We may conclude as a result that the approach in which it is assumed that $\beta_e \neq \beta_c$ is more substantiated.

3.4.2 Reflection of sound from the vapor–liquid interface. We consider the incidence of a sound wave from the vapor phase onto a flat surface of helium II. The vapor is considered to be in a saturation state. The amplitude of pressure oscillations in this wave $\hat{p}_i$ is known, i.e., the vapor pressure is considered to have the value $p_0 + \hat{p}_i$, where p_0 is the unperturbed saturated vapor pressure, thus $p_0 = p_{sat}(T_0)$, where $p_{sat}(T_0)$ is the pressure along the saturation line that corresponds to the unperturbed temperature of the vapor, interface, and liquid T_0.

Due to an increase in pressure, vapor condensation occurs at the interface, and the temperature of this interface begins to increase. After a time interval equal to a half-cycle of the sound wave, the picture changes to the opposite. The vapor pressure turns out to be lowered, $p_0 - \hat{p}_\mathrm{i}$, evaporation of the surface layer of the liquid begins, and the temperature of the interface decreases. A reflected sound wave with amplitude $\hat{p}_\mathrm{r}$ emerges as a result in the vapor, and, in the liquid, a propagating sound wave with amplitude $\hat{p}'_\mathrm{t}$ (the characteristics of the liquid are primed). It is required to determine the amplitude of the sound wave reflected from the interphase surface $\hat{p}_\mathrm{r}$ or the ratio $\hat{p}_\mathrm{r}/\hat{p}_\mathrm{i}$, which we refer to as the coefficient of sound reflection from the liquid–vapor interface.

The mathematical description of the problem is based on a system of equations that represent universal and special consistency conditions at the phase interface [76]. Thus, three conservation equations are formulated for the one-dimensional problem under consideration: for mass, momentum, and energy at the interface; these equations link the corresponding characteristics of the liquid and vapor phases. The linear Labuntsov–Muratova formula obtained by MKT methods is used as a special consistency condition, which allows calculation of the mass flux density during evaporation and condensation for a known interface temperature and vapor pressure. These four equations are supplemented by the relationships between the pressure fluctuations in the incident and reflected waves in vapor and the propagating wave in the liquid (helium II) with the velocities of motion of the vapor and liquid, respectively, in the media under consideration. These equations are derived from Euler's equations of conservation of mass and motion.

The system is closed by an equation that determines the heat flux propagating through helium II as a result of an increase or decrease in the interface temperature. In the process under consideration, due to periodically alternating evaporation and condensation at the interface, which are caused by a periodic decrease and increase in vapor pressure during the incidence and reflection of sound waves, the temperature of the interface changes in a periodic way. Such a change in temperature is a kind of source of a second-sound wave that moves into the bulk of He II. A heat flow propagates along with the second-sound wave, the value of which is determined taking into consideration the positive direction of the coordinate axis from the interface towards the vapor, by the following relation:

$$\hat{q}' = -\rho' a_2 C \hat{T}'_\mathrm{i}\,, \tag{18}$$

where $\hat{q}'$ is the amplitude of oscillations of the heat flux propagating from the interface into the bulk of helium II, ρ' is the density of He II, a_2 is the speed of the second sound, C is the heat capacity of helium II, and $\hat{T}'_\mathrm{i}$ is the amplitude of temperature oscillations of the interface. These oscillations in helium II, in contrast to those in ordinary liquids, are known not to decay as they move into the bulk of the liquid, at least in the nondissipative approximation.

As a result of solving the considered system of equations, the following expression is obtained for the coefficient of reflection of sound R from the surface of helium II that borders the saturated vapor:

$$R = \frac{1 - \chi - 0.86(\rho' - \rho)/(A\rho')}{1 + \chi + 0.86(\rho' - \rho)/(A\rho')}\,, \tag{19}$$

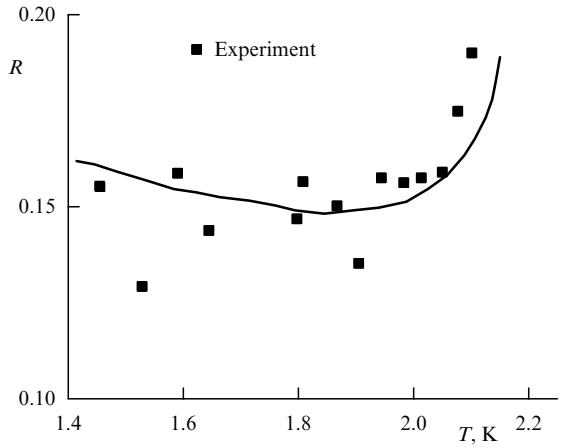

Figure 14. Comparison of calculations with experimental data [69] (squares) on the reflection of a sound wave incoming from vapor to the interface of superfluid helium (He II). R is the coefficient of the reflection of sound from the interface of helium II phases and T is the temperature of this surface. The curve shows the results of our calculations.

where ρ is the helium vapor density,

$$A = 1 + \frac{0.86\,r}{\rho' a_2 C a}\left(\frac{\partial p}{\partial T}\right)_\mathrm{sat}\,,$$

r is the evaporation heat of helium II, a is the speed of sound in helium vapor, $\chi = \rho a/(\rho' a')$ is the reduced wave resistance of the vapor with respect to the liquid, and a' is the speed of the first sound in helium II. The derivative $(\partial p/\partial T)_\mathrm{sat}$ can be found from the Clapeyron–Clausius equation.

A calculation using Eqn (19) shows that, for example, if the temperature of unperturbed He II $T_0 = 2$ K, the sound reflection coefficient $R = 0.15$. The value of R^2 is nothing more than the ratio of the energy fluxes of the reflected and incident sound waves. Since in this case $R^2 \approx 0.02$, it implies that only 2% of the energy flux brought by the incident sound wave is reflected from the interface. The remaining 98% of the incoming energy flow 'passes' into helium II, transforming into waves of the first and second sound. Thus, the interface between the phases of He II–vapor, in contrast to an ordinary liquid, does not really reflect sound, i.e., such a phenomenon as 'echo' is not possible on the 'smooth surface' of superfluid helium.

The calculations made using Eqn (19) are compared with experimental data [69] in Fig. 14. This problem is considered in detail in manual [70], and, for classical liquids, taking into account the nonequilibrium effects on the liquid-vapor interface, in publication [71].

3.4.3 Determination of the recovery load during boiling of helium II. This section presents a technique to calculate the recovery heat flux [72] that was developed in 1980–1981. The so-called noiseless boiling regime is considered, in which the liquid–vapor phase interface is a smooth surface that retains its shape in a stable manner. Along with this type of boiling, a noise boiling regime can be realized in experiments with significant heat loads and large depths of immersion of the heater in He II, in which constant motion of the interface, a change in its shape, and the emergence of an audible sound are observed.

Figure 15 illustrates the location of the heating surface and the vapor and liquid phases during noiseless film boiling.

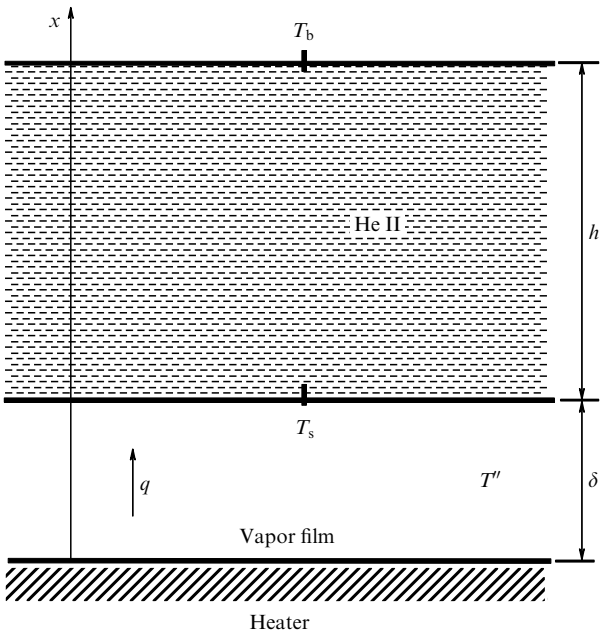

Figure 15. Schematic rendering of noiseless boiling of helium II. A vapor film with thickness δ separates the bulk of superfluid helium from the surface of the heater immersed to the depth h into this liquid. q is the specific heat flux supplied to the lower boundary of the vapor–helium II interface, which has temperature T_s, T'' is the temperature of vapor in the film, and T_b is the temperature of free space of helium II (evaporation surface).

It can be seen that a vapor film separates the heater from the bulk of helium II. We analyze next the processes that occur on a cylindrical heater. In a stationary mode at a certain value of the heat load, i.e., specific heat flux q coming from the surface of the heater, there is a vapor film on this surface with a quite definite thickness δ that does not change with time. An increase in q results in an increase in thickness δ, while a decrease in q leads to a decrease in δ. The film thickness attains the largest value at the maximum value of q equal to the density of the peak heat flux q_p. The specific heat flux in the boiling regime is minimal at a recovery heat load q_R, when the direct contact of the heater surface with helium II is restored, i.e., $\delta \to 0$.

The system of equations necessary to determine q_R is formulated as follows. It follows from the molecular-kinetic description of evaporation–condensation (see Eqn (3) for $\tilde{j} = 0$) that there is a relationship between the vapor pressure near the interphase surface p'' and the specific heat flux arriving at this interface (in this case, q_R), which may be represented as

$$q_R = 2.27\bigl(p'' - p_s(T_s)\bigr)\sqrt{2RT_s}\,, \tag{20}$$

where T_s is the temperature of the liquid–vapor interface, $p_s(T_s)$ is the pressure that corresponds to this temperature along the saturation line, and R is the individual gas constant (for helium $R = 2079\ \mathrm{J\ kg^{-1}\ K^{-1}}$). Formula (20) is valid if the mass flux through the interface is zero. There is no need to substantiate this requirement in the stationary setting under consideration. It should be noted that Eqn (20) is valid at a relatively low intensity of heat transfer when

$$\tilde{q}_R = \frac{q_R}{p_s(T_s)\sqrt{2RT_s}} \ll 1\,.$$

If this inequality is not satisfied, the following formula should be used instead of (20):

$$q_R = 8\left(\frac{p''}{p_s(T_s)} - 1\right)p''\sqrt{\frac{RT_s}{2\pi}}\,, \tag{21}$$

which is obtained from the conservation equations written for a four-moment approximation of the distribution function of vapor molecules over the velocity components. No assumptions about the smallness of the relative heat flux $\tilde{q}_R$ were made in deriving Eqn (21). Equations (20) and (21) take into account the specific features of heat transfer at the interface in the problem under analysis.

Heat transfer across helium II is described by the Gorter–Mellink relation [73], which can be represented in the one-dimensional case in a scalar form:

$$\frac{dT}{dr} = -f(T)\,q^3\,. \tag{22}$$

The heat supplied through the interface propagates further across the liquid (He II). The following equality should be fulfilled for the stationary regime by virtue of the energy conservation law:

$$q_i\,r_i = qr\,, \tag{23}$$

where r is the current radius in the liquid, q is the heat flux density at this distance from the axis of the cylindrical coordinate system, r_i is the radius of the interphase surface, and q_i is the density of the heat flux that enters this surface. Since the mode of restoration of direct contact of He II with the heater is considered, the thickness of the vapor film is $\delta \to 0$; i.e., $r_i = r_s$, where r_s is the heater radius and $q_i = q_R$. Thus, $q = q_R r_s/r$. If this expression for q is substituted into the Gorter–Mellink formula (22), we arrive at

$$\frac{dT}{dr} = -f(T)\,\frac{q_R^3 r_s^3}{r^3}\,, \tag{24}$$

where $f(T)$, q_R, and r_s do not depend on r; therefore, the variables in this equation are separated, which allows us to write

$$\int_{T_s}^{T_\infty} \frac{dT}{f(T)} = -q_R^3 r_s^3 \int_{r_s}^{\infty} \frac{dr}{r^3}\,. \tag{25}$$

We now integrate both sides of formula (25), setting the corresponding limits and taking into account that $T_\infty = T_b$, where T_b is the temperature of He II not perturbed by the heat flux (this is the temperature of the free surface of helium II). As a result, we arrive at

$$T_s - T_b = \tilde{f}(T)\,\frac{q_R^3 r_s}{2}\,, \tag{26}$$

where $\tilde{f}(T) = (T_s - T_b)/\int_{T_b}^{T_s} (1/f(T))\,dT$. The vapor pressure above the free surface of helium II along the saturation line corresponds to the temperature of this surface, i.e., is equal to p_b. The vapor pressure inside the film p'' should be equal in stationary conditions under mechanical equilibrium to the sum of p_b and the hydrostatic pressure, the value of which is determined by the depth h to which the heater is immersed in He II:

$$p'' = p_b + \rho g h\,, \tag{27}$$

where g is the acceleration of gravity.

For given T_b, h, and the known dependence of the saturation pressure of helium on temperature, the system of three equations, (20), (26), and (27), contains three unknown quantities, q_R, p'', and T_s, which can be found by solving this system. The surface temperature of the liquid (He II) T_s in contact with the vapor film may vary, depending on the depth to which the heater is immersed in helium II, from T_b to $T_b + (dT/dp)_{sat}\,\rho gh$.

The solutions to the problem obtained by the method described above show that the temperature of the He II interface for small diameters of heaters is close to T_b, and for large ones, to $T_b + (dT/dp)_{sat}\,\rho gh$. It follows from Eqn (20) that the value of the recovery heat flux q_R at small diameters should be higher, since $p_s(T_b) < p_s(T_b + (dT/dp)\rho gh)$. It should be noted that in the formulation of the problem under consideration the vapor pressure p'', by virtue of (27), only depends on the pressure p_b above the free surface of helium II and the heater immersion depth h. A comparison of the calculated data to the experimental results presented in [72] shows that agreement is better at small heater diameters, i.e., when the thermal resistance in the liquid is relatively small, and the efficiency of heat transfer is driven by processes that occur at the interface between helium II–vapor phases.

The considered approach was used later to determine the recovery heat loads in experiments on the boiling of superfluid helium on the surface of spherical heaters 4.8 and 6.0 mm in diameter [74]. Good agreement was obtained between the calculated and experimental results for the spherical geometry.

It should be noted at the end of this section as a summary of the experimental studies in which the condensation coefficient was determined that its value is close in the first approximation to unity. This conclusion may be based on the results of [56, 77] for the condensation of mercury and potassium vapor [57, 78], intense evaporation of iodine [60, 61], supersonic air condensation [65], and reflection of sound from the interface of superfluid helium [66–68]. The same conclusion follows from reviews of the condensation coefficients for water [4, 79], since this is quite explicitly asserted in [79], while it can be seen from [4] that a significant dispersion of experimental data on the condensation coefficient of water is apparently due to the fact that the measurements were made under different conditions. Smaller values were obtained in an indirect way and at a distance from the interface that was significant compared to the average mean free path of vapor molecules. If this circumstance is taken into account, the conclusion that the water condensation coefficient is close to unity becomes substantiated.

4. Condensation from a vapor–gas medium

The problem of evaporation and condensation from a vapor–gas mixture is more involved than analogs for a one-component medium; indeed, in the molecular-kinetic approach, it is necessary to solve not one, but two kinetic Boltzmann equations, which contain four collision integrals. Consequently, finding the solutions becomes a more challenging task, and the time needed to obtain them increases. However, the problem itself is more interesting, also from the perspective of basic studies, since it enables unknown features of the behavior of such systems to be discovered. This problem is also of importance for applied research, since most processes of transfer through interfaces implemented in practice occur specifically in the contact of the condensed phase with a vapor–gas mixture, for example, the evaporation of water into air.

Transfer processes occur in many heat and mass exchangers and devices, which are due to the evaporation of a liquid at a certain temperature, the movement of the formed vapor through the vapor–gas mixture, and the condensation of this vapor on the surface, the temperature of which is maintained lower than that of the evaporation surface. Phenomena of this kind take place during the drying of various bodies, the formation of protective coatings for elements of power generation equipment, the distillation of substances under conditions of reduced pressure (vacuum distillation, chemical vapor deposition), etc. It is noted in today's publications on this topic that the exploration of condensation–evaporation processes in the presence of a noncondensable component is important for the development of technologies for storage and transportation of cryogenic fuel, both on earth and in space. Consequently, finding the conditions for efficient condensation of vapor from a vapor–gas mixture is a very important task in studying the corresponding processes of heat and mass transfer and the design and development of engineering devices intended for various purposes.

It is well known that the presence of a noncondensable component in a vapor–gas mixture reduces the intensity of condensation to such an extent that a kind of blocking of the condensing surface occurs in a number of cases, i.e., vapor ceases to condense at all. It is clear that finding such conditions is very important for the design and development of various types of condensers.

It is generally believed that vapor is 'delivered' to the surface due to diffusion, and the phase interface is impermeable to gas, i.e., the gas mass flux is zero, $j_g = 0$. It should be noted that the diffusion model is strictly valid for low concentrations of vapor or gas. Using the condition that the mass flux density of the noncondensable gas is zero, i.e., $\rho D\,dC_g/dx - \rho C_g u_x = 0$, the following formula may be derived for the mass flux density of the condensing substance:

$$j_v = \frac{\rho D}{L} \ln\left(\frac{1 - C_v(x = L)}{1 - C_v(x = 0)}\right). \tag{28}$$

Here, $C_v = \rho_v/\rho$ is the relative partial density, ρ_v is the vapor density, ρ is the density of the entire mixture, D is the coefficient of mutual diffusion, j_v is the vapor mass flux density, and L is the size of the region under study.

It should be emphasized that the use of a purely diffusion approach to condensation or evaporation is not always justified. As a result of the evaporation of substance, the noncondensable component (gas) is apparently 'driven away' by the vapor moving from the interface. Situations are possible where the gas content in the system is small, while the evaporation rate is quite high to completely 'drive the gas away' from the interface. The relative partial density near the evaporating surface tends in this case to unity, i.e., $C_v(x = 0) \to 1$. Formula (28) is not applicable in such a situation and, as a consequence, calculations should be made using alternative approaches. However, another limiting case can also be realized, when the pressure of the noncondensable component is much higher than the vapor pressure. The process of cryopumping of water vapor through a region filled with gaseous argon was studied in [80].

The argon pressure in the systems under consideration ranges from 0.5×10^{-3} Torr to 20.0×10^{-3} Torr, while the water vapor pressure is several orders of magnitude lower,

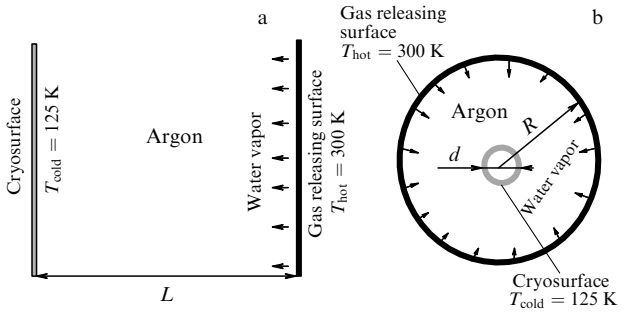

Figure 16. Cryopumping of water vapor through a region filled with gaseous argon. Two implementations of recondensation of water vapor through the volume occupied by gaseous argon are shown: for (a) planar and (b) cylindrical geometries. Water vapor is supplied from a surface that has a temperature $T_{hot} = 300$ K, passes through a layer of gaseous argon, and condenses (desublimates) on a cryosurface whose temperature is $T_{cold} = 125$ K. L is the distance between the surface that releases the water vapor and the cryosurface in the case of planar geometry, R is the radius of the surface that releases gas, and d is the diameter of the cryosurface for the cylindrical geometry.

being $10^{-8}-10^{-6}$ Torr. The flows of the noncondensable component (argon) in such systems correspond to the transient or viscous flow regime. The setup of the problem is shown in Fig. 16 for rectangular and cylindrical interfaces.

Water vapor enters the system from a 'hot interface' (gas-releasing surface in Fig. 16); the rate of gas release from the surface is considered to be known and is determined by the material from which surfaces that limit the area under study are made. It is usually assumed that water vapor released from the surface is delivered to the opposite surface due to diffusion and condenses there (cryosurface in Fig. 16). However, the use of this diffusion approach does not enable experimentally observed data to be obtained. For example, if the argon pressure is $P_{Ar} = 2 \times 10^{-3}$ Torr, the argon density, respectively, is $\rho_{Ar} = 4.27 \times 10^{-6}$ kg m^{-3}. As noted above, the water vapor pressure is several orders of magnitude lower: $P_{H_2O} = 10^{-6}$ Torr; therefore, the density of water vapor is $\rho_{H_2O} = 0.96 \times 10^{-9}$ kg m^{-3}. Thus, the density of the mixture $\rho \approx \rho_{Ar}$. As a consequence,

$$C_{H_2O} = \frac{\rho_{H_2O}}{\rho} \approx \frac{0.96 \times 10^{-9}}{4.27 \times 10^{-6}} .$$

If $C_{H_2O} \ll 1$, we obtain then from Eqn (28)

$$j_v = \frac{\rho D}{L}\left(C_{H_2O}(0) - C_{H_2O}(L)\right) . \qquad (29)$$

The experimentally observed mass flux density of water vapor is 10^{-8} kg m^{-2} s^{-1}. Equation (29) may be used to determine what difference in relative densities is necessary to obtain such a value of the mass flux density, i.e.,

$$C_{H_2O}(0) - C_{H_2O}(L) = \frac{j_v L}{\rho D} . \qquad (30)$$

The size of the area under investigation is $L = 0.914$ m, and the diffusion coefficient is $D \approx 3 \times 10^{-5}$ m^2 s^{-1}. Further, it follows from (30) that $C_{H_2O}(0) - C_{H_2O}(L) = 71.35$. Since the relative density is by definition less than unity, the obtained values of $C_{H_2O}(0)$ and $C_{H_2O}(L)$ cannot be realized. Thus, the use of the diffusion approach does not allow obtainment of experimentally observable results.

It turns out that the problem of cryopumping of water vapor through an argon medium may only be solved and the dependence of the pressure on the distance to the cryopanel be determined using the molecular kinetic approach [80]: the Knudsen numbers for argon and water vapor under the considered conditions are fundamentally different: $3.0 \times 10^{-3} < \mathrm{Kn}_{Ar} < 2.0$, $\mathrm{Kn}_{H_2O} \gg 1$, i.e., the state of argon is close to continuous, while that of water is close to free-molecular. The corresponding results and the calculation technique are presented in [80]. However, to apply this method in the entire domain under study at low Knudsen numbers for both components, significant computer resources are required. It is proposed to use in this case a 'matching' approach, in which the outer region is described using the equations of gas dynamics, while the near-surface Knudsen layer is described by kinetic methods. Thus, there are three options to describe condensation from a vapor–gas mixture. In the first, most general, approach, the system of kinetic equations is solved in the entire domain of computations. The second option is based on the 'matching' technique. In the third, most approximate, approach, results of the corresponding solution for a one-component medium may be used. It is clear that the last option has a narrower field of application, which is limited by the available 'one-component' results.

A solution to the system of two kinetic Boltzmann equations in the entire computational domain was obtained in [81] for the problem of recondensation in the presence of a noncondensable component for the Knudsen numbers for vapor equal to 0.5, 0.1, and 0.01. The method of direct numerical solution was used to this end [82]. Good agreement with the results obtained in [83] by the adapted Direct Simulation Monte Carlo (DSMC) method has been shown. Proposed and implemented in [81, 84] was a technique for calculating essentially nonequilibrium flows of three-component mixtures, for which the collision cross sections and masses of the components differ by several orders of magnitude. The technique developed is based on the application of method [82]. This approach was used to investigate recondensation during the movement of vapor through a gas–dust mixture, taking into account evaporation and condensation on the surfaces of particles (dust grains, drops, clusters) with a relatively large size and mass. A solution was found in [85] for a system of two kinetic Boltzmann equations for the problem of droplet evaporation in a vapor–gas medium at a large ratio of the gas and vapor densities. The real situation of water evaporation at room temperature into the ambient air was considered.

We discuss next the second ('matching') and third ('quasi-continuous') approaches to the description.

4.1 Conjugation of solutions of a system of kinetic and gas-dynamic equations

The method of joint solution of the Boltzmann kinetic equation (BKE) and the CM equations enables, on the one hand, the Navier–Stokes equations to be 'provided' with the correct boundary conditions that take into account non-equilibrium singularities near the interfaces, and, on the other hand, a significant reduction in computation time.

In using this approach, the kinetic region, i.e., the domain in which the problem is solved using a single BKE or a BKE system (for a mixture of gases), is located directly near the interface, and its thickness is several free paths of vapor (or gas) molecules.

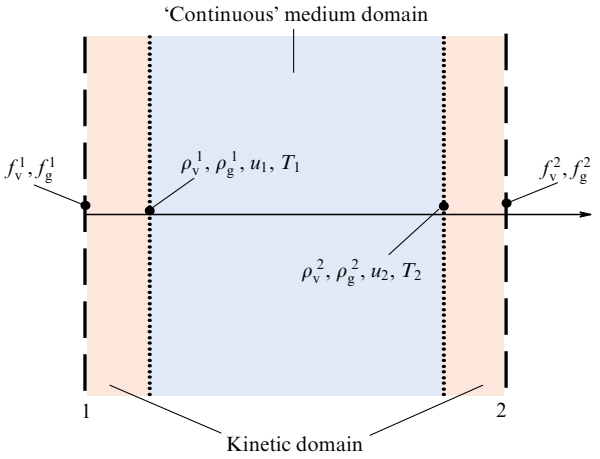

Figure 17. Combined method of solving a system of kinetic and gas-dynamic equations for an evaporation–condensation problem. The solution is found in the kinetic region using the MKT methods for gases (in terms of the velocity distribution of molecules), while in the continuum medium, the CM system of conservation equations is employed.

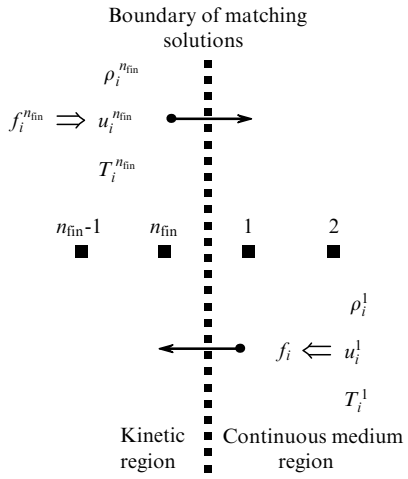

Figure 18. Illustration of the matching procedure. The flow macroparameters in the kinetic region are determined from the solution of a single Boltzmann kinetic equation or a system of such equations. The quantities from the last calculated point n_{fin} in the kinetic region, i.e., $\rho_i^{(n_{fin})}$, $u_i^{(n_{fin})}$, and $T_i^{(n_{fin})}$, are used as boundary conditions for the equations of continuum mechanics. Used as a boundary condition for the BKE at the boundary of the matching of the solutions is the Chapman–Enskog DF with the parameters from the first computational point of the 'continuous medium region': ρ_i^1, u_i^1, T_i^1, i.e., $f_i = f(\rho_i^1, u_i^1, T_i^1)$.

The rest of the semi-space is the region of a 'continuous' medium, in which the solution is found using the system of conservation equations for the mechanics of a continuous medium (Fig. 17, where the subscripts v and g refer to vapor and gas, respectively).

If the degree of rarefaction of a gas is relatively small, i.e., the Knudsen number is much less than unity, the behavior of the gas may be described without going into the details of molecular interactions. Consequently, the deviations from local thermodynamic equilibrium are small far from the phase interfaces, and the conservation equations can be used to describe heat and mass transfer. It is known at the same time that for small Knudsen numbers the DF is close to the Chapman–Enskog function, which, in the absence of heat flux and viscous stresses, transforms into the Maxwell distribution. Thus, the entire domain under investigation may be schematically divided into a 'kinetic' region, which is directly adjacent to the interface, and a region of a 'continuous' medium, which is separated from the interface by a distance of several average mean free paths of gas (vapor) molecules. At the boundary between the kinetic region and the 'continuous'-medium region, solutions are 'matched'. This procedure is schematically illustrated in Fig. 18. Both domains are separated by a conventional border, indicated in the figure by a dashed line.

As noted above, the flow parameters of the 'kinetic region' are determined from the solution of one BKE (for pure vapor or gas) or the BKE system (for a mixture). The algorithm to solve the Boltzmann kinetic equation assumes that to do so the velocity distribution function of molecules 'flying' into the kinetic region from the region of a continuous medium must be known. This function is denoted in Fig. 18 as f_i, where $i = \mathrm{v}, \mathrm{g}$ for a two-component mixture and $i = \mathrm{v}$ (or g) for a one-component medium.

Used as such an input is the Chapman–Enskog function with parameters from the first point of computation in the 'continuous medium region' $f_i^1 = f(\rho_i^1, u_i^1, T_i^1), i = \mathrm{v}, \mathrm{g}$. This function for a one-dimensional flow may be represented as follows:

$$f_i^1 = f_M \left[1 - \frac{\tau_{xx}}{2p}\frac{c_x^2}{RT} - \frac{q_x}{p}\frac{c_x}{RT}\left(1 - \frac{1}{5}\frac{c^2}{RT}\right)\right], \qquad (31)$$

where f_M is the Maxwell distribution function calculated using the parameters at point 1,

$$f_M^1 = \frac{n_1}{(2\pi RT_1)^{3/2}} \exp\left[-\frac{(\xi_x - u_1)^2 + \xi_y^2 + \xi_z^2}{2RT_1}\right], \qquad (32)$$

c_x is the projection of the relative velocity of the molecule on the x axis,

$$c_x = \xi_x - u_1\,, \qquad (33)$$

τ_{xx} is the viscous strain,

$$\tau_{xx} = \frac{4}{3}\mu\frac{\partial u}{\partial x} \approx \frac{4}{3}\mu(T_1)\frac{u_2 - u_{fin}}{2\Delta x}\,, \qquad (34)$$

and q_x is the heat flow,

$$q_x = -\lambda\frac{\partial T}{\partial x} \approx -\lambda(T_1)\frac{T_2 - T_{fin}}{2\Delta x}\,. \qquad (35)$$

The pressure p and temperature T in (31) are equal to the corresponding parameters at point 1 at the nth time step.

The solution of the kinetic equation is used to determine the velocity distribution function of molecules at each point of computation in the 'kinetic domain'. The function obtained is then used to calculate in this region the macroparameters of the mixture, including the macroparameters at the point n_{fin}, i.e., $\rho_{fin}, u_{fin}, p_{fin}$, and T_{fin} (see Fig. 18). Next, the system of conservation equations for the continuous medium is solved, the boundary conditions for these equations being the macroparameters previously found at the point n_{fin}.

It should be noted that, in performing calculations using the matching of solutions, negative values of function (31) may emerge. This may be due to an incorrect choice of the boundary where the solutions are matched. To eliminate this defect, the kinetic domain should be extended by shifting this boundary to the region of a continuous medium.

An important condition for obtaining smooth conjugation of the solutions is the exact equality of the fluxes of mass,

momentum, and energy across the boundary where the solutions are matched. In performing the numerical integration of function (31) (Chapman–Enskog), the requirement of exact equality of flows is not satisfied. To fulfill this condition, the f_M function is corrected in the following way: the macroparameters n, T, u in f_M are replaced by close parameters n^*, T^*, and u^* obtained as a result of the iterative procedure.

Thus, the combined solution of the conservation equations and the Boltzmann equation consists of the following operations.

(1) The solution of the conservation equations at the previous step in time (at the first step, initial conditions) is used to determine the distribution functions of the molecules that move out of this region.

(2) The Boltzmann equation is solved in the regions close to the interface (evaporation or condensation surface).

(3) The solution of the Boltzmann equations is used to find the macroparameters of the vapor at the boundaries of the computation regions.

(4) The equations of conservation of mass, momentum, and energy are solved in the continuous medium region.

We consider as an example a one-dimensional semi-infinite problem of condensation of vapor on an interface. The condensed-phase temperature is T_s, and the coordinate of this surface $x = 100$. The gas in the $0 < x < 100$ region has at the initial moment pressure p_∞, temperature T_∞, and velocity u_∞.

Solutions to the nonstationary problem for various values of the Mach number are displayed in Figs 19–21. The profiles of macroparameters (density, temperature, and velocity) at various times for subsonic condensation (Mach number $M_\infty = 0.109$) are shown in Fig. 19a, and the results for supersonic condensation (Mach number $M_\infty = 1.09$) are shown in Fig. 19b. The condensation surface is located at the coordinate $x = 100$. The values are displayed in Figs 19–21 in dimensionless form. The pressure and temperature of the gas at infinity (p_∞, T_∞) are used as the baselines to reduce the parameters to a dimensionless form, and the speed of sound at infinity a_∞ is employed as the velocity scale. In the figures, p_s is the vapor pressure that corresponds to the temperature of the condensed phase, i.e., $p_s = p(T_s)$.

Figure 20 compares the results obtained in the matching approach with the solution to a model BKE (the Bhatnagar–Gross–Krook (BGK) model) [86]. The results of the matching approach are shown by curves, while the solutions to the model BGK equation are displayed as squares, triangles, and dots.

Figure 21 shows the stationary solution to the problem of subsonic condensation with the Mach number $M_\infty = 0.34$.

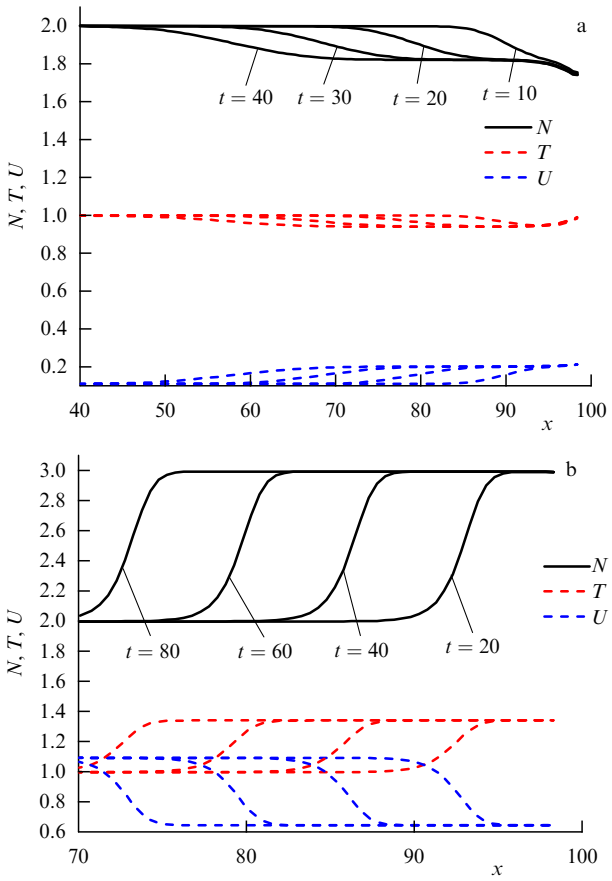

Figure 19. Coordinate dependences of macroparameters (numerical density N, temperature T, and velocity U) for various time points in the problem of nonstationary condensation of vapor on a planar surface obtained using the matching method at $p_\infty/p_s = 2$. The condensation surface is located at the coordinate $x = 100$. The parameters of the gas at the initial moment in the range from $x = 0$ to $x = 100$ are as follows: pressure p_∞, temperature T_∞, and velocity u_∞. The temperature of the condensation surface is T_s. (a) Subsonic condensation, $M_\infty = 0.1095$; (b) supersonic condensation, $M_\infty = 1.095$.

4.2 Description of vapor condensation through a vapor–gas mixture using an approximate kinetic solution for a one-component medium

We now consider the one-dimensional stationary problem of condensation from a vapor–gas mixture in the following formulation [87]. The system contains a certain amount of gas (noncondensable component). The temperature of the interface and the pressure and density that correspond to this temperature along the saturation line are known. A vapor flow is supplied to this condensation surface from afar. Similar to condensation of pure vapor, which is considered in Section 3, two gas-dynamic quantities, for example, the density and temperature of the oncoming vapor flow, are assumed to be known far from the interface. It is required that the distribution of density and temperature along the coordinate and the mass flux density of the condensing vapor be found. Since a vapor–gas mixture is considered, it is of importance to determine, among other things, at what amount of gas the vapor condensation on the cooled surface is at all possible.

The presented problem is described in the mechanics of continuous media by four conservation equations: three equations of conservation of mass, momentum, energy for the mixture as a whole and the equation of conservation of the mass of the component. The solution to the system of three equations of conservation of mass, momentum, and energy obtained for pure vapor at a Prandtl number of $\mathrm{Pr} = 3/4$ [54] is in this case also valid for the entire mixture, since only vapor flows from afar. Therefore, information additional to this solution can be obtained from the equation of conservation of the mass of a component, gas or vapor. The latter can be represented as follows:

$$j = \rho_v u - \rho D \frac{\mathrm{d}C_v}{\mathrm{d}x}\,, \tag{36}$$

where ρ_v is the vapor density, ρ is the density of the mixture, u is the velocity of its movement, D is the coefficient of mutual diffusion of vapor and gas, $C_v = \rho_v/\rho$ is the relative partial

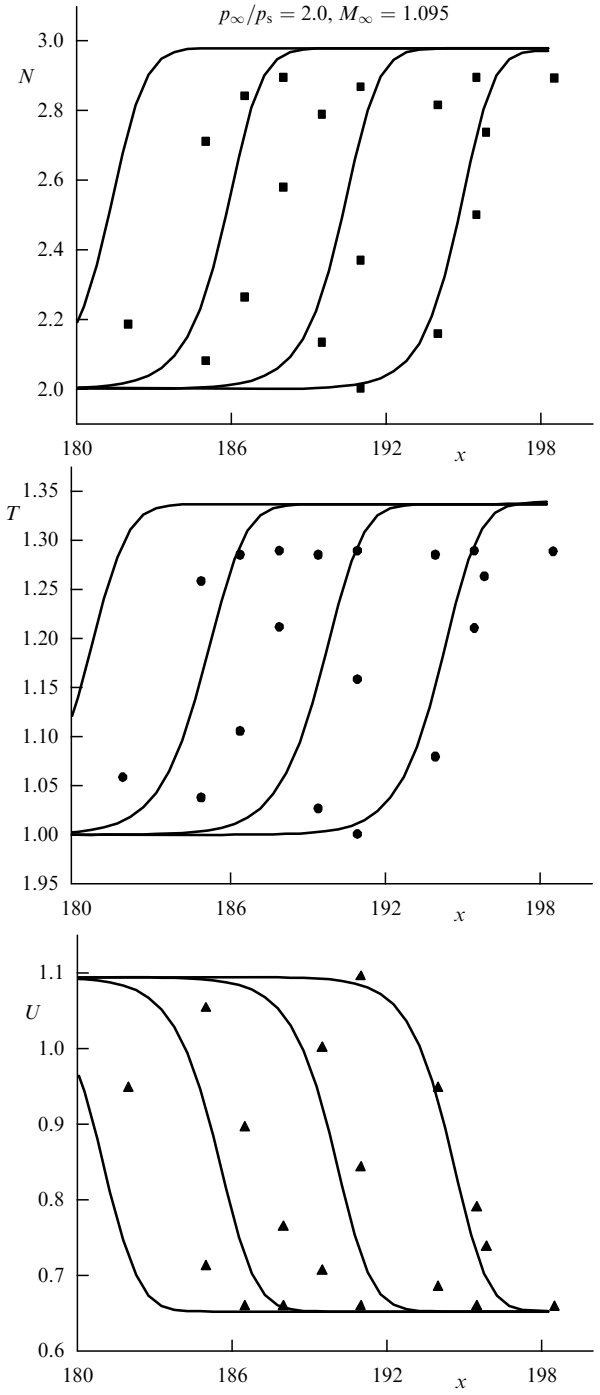

Figure 20. Comparison of solutions to the nonstationary problem of supersonic condensation ($M_\infty = 1.095$) on a planar surface at $p_\infty/p_s = 2$ obtained by the matching method and by solving a model BGK equation [86]. Similar to the case displayed in Fig. 19, the parameters of the gas (pressure p_∞, temperature T_∞, and velocity u_∞) are considered to be specified.

vapor density, x is the coordinate along the axis normal to the interphase surface, and j is the vapor mass flux density (in the considered one-dimensional stationary formulation, this value is constant). Consequently, the solution of Eqn (36) with the Lewis–Semyonov number equal to one, Le = 1, has the form

$$C_v(x) = 1 - \exp\left(\frac{3j}{4}\int_0^x \frac{dx}{\mu}\right)\left[1 - C_v(0)\right], \tag{37}$$

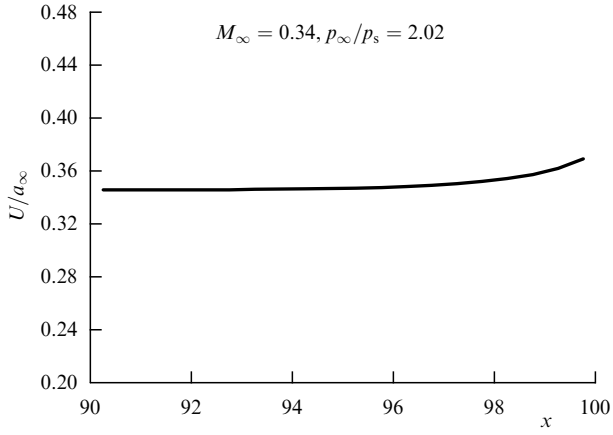

Figure 21. Solution to the problem of subsonic condensation on a planar surface at the stationary stage obtained using the matching method. The condensation surface is located at the coordinate $x = 100$.

where μ is the dynamic viscosity of the mixture. By definition, Le $= D/a$, where a is the thermal diffusivity of the mixture.

Thus, if the specification of two gas-dynamic quantities, as in the case of condensation of pure vapor, makes it possible to calculate the mass flux density j, Eqn (37) allows obtainment of the sought-after dependence of the partial gas density on the coordinate for the value of this quantity set at $x = 0$. The equality $C_v(0) = 0$ determines the maximum possible condensation mode, since any further increase in the amount of gas should lead to a negative vapor density. For this case, i.e., for $C_v(0) = 0$, Eqn (37) takes the form

$$C_g^{\lim}(x) = \exp\left(\frac{3j}{4}\int_0^x \frac{dx}{\mu}\right). \tag{38}$$

Formula (38) may be used to calculate the largest (blocking) amount of gas in the mixture. Condensation is only possible in this setup until the inequality

$$\int_{-\infty}^{0} \rho_g\, dz \leqslant \int_{-\infty}^{0} \rho_g^{\lim}\, dz \tag{39}$$

holds valid, where $dz = (3/4)(j/\mu)\,dx$. It follows from Eqn (38), given that $C_g^{\lim} = \rho_g^{\lim}/\rho$, that

$$\frac{\rho_g^{\lim}}{\rho} = \exp\left(\frac{3j}{4}\int_0^x \frac{dx}{\mu}\right), \quad \text{i.e.,} \quad \rho_g^{\lim} = \rho \exp\left(\frac{3j}{4}\int_0^x \frac{dx}{\mu}\right).$$

If we substitute into Eqn (39) the density $\rho_g^{\lim}$ obtained in this way, where ρ is found from the solution of equations of conservation of mass as $\rho = \rho_\infty u_\infty/u$, and u/u_∞ is determined from the solution of the equation of conservation of momentum for the one-component medium [54], we arrive at

$$\int_{-\infty}^{0} \rho_g\, dz \leqslant \rho_\infty \int_{-\infty}^{0} \frac{\exp z}{1 + a_1 \exp z}\, dz, \tag{40}$$

where a_1 is the coefficient in the aforementioned equation of motion [54], $u/u_\infty = 1 + a_1 \exp z$, u is the velocity of vapor in the cross section z, and u_∞ is the velocity of vapor at $z \to -\infty$. Integration of the right-hand side of Eqn (40) gives

$$\int_{-\infty}^{0} \rho_g\, dz \leqslant \frac{\rho_\infty}{a_1} \ln|1 + a_1|. \tag{41}$$

The same transformations for Le = 3/4 yield the following expressions, which differ from formulas (37), (38), (40), (41)

Table 3. Quantities calculated for limiting condensation regimes.

a_1	$\frac{\int_{-\infty}^{0}\rho_g\,dz}{\rho_\infty}\leqslant 1$, Le = 1	$\frac{\int_{-\infty}^{0}\rho_g\,dz}{\rho_\infty}\leqslant 1$, Le = $\frac{3}{4}$
−0.162	1.09	0.84
0.195	0.91	0.68
−0.134	1.07	0.83
0.043	0.98	0.80
−0.189	1.11	0.85
−0.127	1.07	0.83
−0.087	1.05	0.81
0.039	0.98	0.81
0.137	0.94	0.71
−0.013	1.00	1.23

obtained for Le = 1:

$$C_v(x) = 1 - \exp\left(j\int_0^x \frac{dx}{\mu}\right)\left[1 - C_v(0)\right], \tag{42}$$

$$C_v^{\lim}(x) = 1 - \exp\left(j\int_0^x \frac{dx}{\mu}\right), \tag{43}$$

$$\int_{-\infty}^{0}\rho_g\,dz \leqslant \rho_\infty\int_{-\infty}^{0}\frac{\exp(4z/3)}{1+a_1\exp z}\,dz, \tag{44}$$

$$\int_{-\infty}^{0}\rho_g\,dz \leqslant \frac{\rho_\infty}{a_1}\left[3 - \frac{\ln|1+a_1^{1/3}|}{a_1^{1/3}} + \frac{1}{2a_1^{1/3}}\ln\left|\left(a_1^{1/3}-\frac{1}{2}\right)^2+\frac{3}{4}\right| - \frac{\sqrt{3}}{a_1^{1/3}}\arctan\left(\frac{\sqrt{3}\,a_1^{1/3}}{2-a_1^{1/3}}\right)\right]. \tag{45}$$

Calculations of the right-hand sides of inequalities (41) and (45) for the solutions $u/u_\infty = 1 + a_1\exp z$ are presented in Table 3, wherein the values of a_1 are taken from [54].

The above description is developed, as for pure vapor, with consideration for the compressibility of the condensed medium, implying that both the density of the mixture and the density of its individual components (vapor and gas) may vary along the coordinate. The faster the vapor flow moves, the stronger the noted compressibility is manifested. On the contrary, if Mach numbers for this flow are low, the density of the vapor–gas mixture may be considered in the first approximation to be constant. Condensation from a vapor–gas mixture in this approximation is considered, for example, in monograph [88].

To analyze the calculated quantities, we emphasize that, as per the formulation of the problem, a vapor flow is continuously supplied to the working volume through the right inlet section and, having passed through a layer of a binary vapor–gas mixture, it successfully condenses on the left section of the system. The system initially contains some amount of gas. Solutions (41) and (45) make it possible to determine the largest values of this amount, at which, in principle, one-dimensional stationary condensation is possible. If the amount of gas in the system is larger, it will prevent the entire incoming vapor from reaching the interface and successfully condensing on it. The vapor mass flux density will be in this case less than the value that corresponds to the given values of the density and temperature of the vapor at the inlet. As a result, the vapor density in the inlet section should increase, while, according to the formulation of the problem, it is considered given ab initio. In another real setup, in which the vapor temperature in the inlet section T_∞ and the vapor mass flow density j are known, the solution of the momentum conservation equation [54] enables determination of the vapor density in this section ρ_∞ that corresponds to the given T_∞ and j. If the maximum amount of gas is exceeded, the system will not be able to maintain this value of ρ_∞; consequently, the mass flux density j must also be different, while initially it is assumed to be given.

The one-dimensional setting, apparently, is the most rigid, since the gas has no way to escape under the pressing action of the oncoming vapor. It can only collect near the interface, thereby preventing condensation and eventually resulting, under some of the conditions considered above, in the complete termination of the removal of vapor from the system. Two-dimensional and three-dimensional settings may be more 'liberal' in this sense, since the gas can move away from the condensation surface in a tangential direction. However, if the system is closed, then, when a certain initial amount of gas is exceeded in it, conditions for blocking the condensation surface will eventually also emerge in multi-dimensional problems. These conditions depend on the relationship between the condensing and vapor-impermeable surfaces, their temperatures, etc., but it is unlikely that the blocking amount of gas will be less than the estimate made for the one-dimensional setting. Consequently, it may be assumed that, if inequality (39) is satisfied in designing a condenser, such a device will be able to provide the designed condensation rate j determined by ρ_∞ and T_∞.

Consequently, vapor will successfully condense in the system under consideration with the same mass flux density j for various amounts of gas in the system. The only condition of importance is that this quantity not exceed the value determined by inequality (39). The distributions of the density and temperature of the mixture along the coordinate, which do not depend in this case on the amount of gas the system initially contained, are determined by solutions of the momentum conservation equation [54]. An increase in the amount of gas from zero (condensation of pure vapor) to a limiting value only leads to a redistribution of partial densities. The density of the mixture near the interface in the absence of gas is exactly equal to the vapor density. However, in approaching the blocking regime, the vapor density at the interface decreases, while the gas density increases. It should be kept in mind that, according to the formulation of the 'semi-infinite' problem under consideration, the mass concentration of vapor far from the interface is always equal to unity, i.e., vapor alone rather than the mixture is supplied to the system. If the density and temperature of the components in a one-dimensional stationary problem are required to be constant far from the interface, it cannot be otherwise, since the interface does not allow gas to pass through. If the mixture rather than pure vapor were continuously inflowing, the density ρ_g and the pressure P_g of the gas would inevitably increase in time, and the flow region wherein the gradients ρ_g and P_g are different from zero would shift in the positive direction of x. The specific dependence of the vapor density on the coordinate is determined by solution (37). The quantity $C_v(0)$ that this formula contains may be estimated for the known initial amount of gas in the system $\int_z^0 \rho_g^{in}\,dz$ using the following relations:

$$C_v(0) = 1 - C_g(0), \tag{46}$$

$$C_g(0) = \frac{\rho_g(0)}{\rho_\infty}, \tag{47}$$

$$\frac{\rho_g(0)z}{2} = \int_z^0 \rho_g^{in}\,dz\,. \quad (48)$$

It can be seen from Eqn (37) that the mass concentration of vapor increases most sharply with an increase in the coordinate at low values of this concentration near the interface. Consequently, the mass concentration of the gas sharply decreases in this case. The density of the mass flux of the condensing substance j is defined in the MKT as the difference between two oppositely directed molecular fluxes: the flux of molecules j^+ moving from the interface (as a result of evaporation) and the flux of molecules j^- moving to the interface. As the interface temperature decreases, the flux of evaporating molecules j^+ decreases and, as a consequence, the resulting condensation flux j increases. Thus, an increase in the intensity of the process for a pure substance may be achieved by lowering the temperature of the interface. On the other hand, if the region under study contains a noncondensable gas, the main 'resistance' to movement of vapor is due precisely to collisions with the molecules of this gas. The flow of vapor molecules to the condensation surface is blocked by frequent collisions with noncondensable gas molecules. Moreover, even if the conditions for condensation are improved by lowering the temperature of the interface, the required mass flux density of the condensed substance cannot be attained in this case (and this is the difference from the case of a pure substance).

The approach presented above does not take into account the specific features of collisions between vapor and gas molecules that occur in the immediate vicinity of the interface in the Knudsen layer. To obtain more accurate estimates of the effect of the noncondensable component on the features of condensation, it is necessary to use the kinetic description. Simulations of this kind were carried out in [89], where it was also assumed that far from condensation surface vapor alone is located. To find the parameters of the mixture and each of the components, a model kinetic equation for gas mixtures was used. The temperature of the phase interface, the vapor density far from it, and the Mach number of the incoming vapor were considered to be given. The solution yields distributions of the macroparameters of the mixture for various initial gas contents in the system. The authors of [89] note that situations may occur in which the gas present near the condensation surface prevents the movement of vapor, which leads to the termination of condensation. Such results were obtained for several values of the Mach number. For example, calculations for $M_\infty = 0.1$ have shown that one-dimensional stationary condensation of vapor that passes through a vapor–gas mixture becomes impossible if $\int_0^\infty \rho_g\,d(x/l_\infty) \geqslant 9.0\rho_\infty$, even at an arbitrarily low temperature of the interface. This feature near the phase interface is due to the blocking effect of the gas, which does not allow vapor to pass to this interface in the required amount.

Using kinetic calculations [89], it is easy to assess the correctness of the evaluation procedure considered above. It follows from Table 3 that $\int_{-\infty}^0 \rho_g\,dz \leqslant \rho_\infty$. Since

$$dz = \frac{3}{4}\frac{j}{\mu}\,dx\,, \quad j = \rho_\infty u_\infty\,, \quad \mu \approx \frac{1}{3}\rho_\infty l_\infty \sqrt{\frac{8RT_\infty}{\pi}}\,,$$

then

$$dz = \frac{9}{8}\frac{\rho_\infty u_\infty \sqrt{\pi}}{\rho_\infty l_\infty \sqrt{2RT_\infty}}\,dx\,.$$

The Mach number for a monatomic gas is

$$M_\infty = \frac{|u_\infty|}{\sqrt{(5/3)\,RT_\infty}}\,.$$

Hence,

$$dz = \frac{9}{8}\frac{u_\infty}{\sqrt{(5/3)RT_\infty}}\,d\left(\frac{x}{l_\infty}\right)\sqrt{\frac{5\pi}{6}} = -1.82M_\infty\,d\left(\frac{x}{l_\infty}\right).$$

In this way,

$$\int_{-\infty}^0 \rho_g\,dz = 1.82\int_0^\infty \rho_g M_\infty\,d\left(\frac{x}{l_\infty}\right).$$

For a Mach number equal to 0.1, we obtain

$$1.82\int_0^\infty \rho_g 0.1\,d\left(\frac{x}{l_\infty}\right) \leqslant \rho_\infty\,.$$

This implies that, for $\int_0^\infty \rho_g\,d(x/l_\infty) \geqslant 5.5\rho_\infty$, condensation of vapor passing through the vapor–gas mixture becomes impossible. Thus, an accurate kinetic calculation shows that, if the initial gas content in the system is greater than $9.0\rho_\infty$, then condensation with a velocity of $M_\infty = 0.1$ will not occur. The simplified approach indicates at the same time that condensation with such a Mach number terminates if the gas content in the system exceeds $5.5\rho_\infty$.

The following conclusion may be drawn as a result. The 'one-component' method presented in [54] to describe the condensation of a vapor–gas mixture enables determination of the limiting amount of gas in the system at which vapor condensation on the surface is at all possible. In solving this problem, there was no need to resort to the MKT methods. It was sufficient to employ the known results of the application of such methods to studies of a one-component system (pure vapor) and to solve the equation of conservation of mass of a continuous medium component. This is due to the accurate formulation of the boundary condition for the gas at the interface owing to its impermeability for this component.

Approach [54] was developed in [90] for vapor condensation in the presence of a noncondensable component. The authors of [90] presented their results as a formula that generalizes Eqn (7) (Section 2.2.2), applicable in the range of the ratio of molar masses of components $0.03 \leqslant \mu_g/\mu_v \leqslant 1.24$ and the corresponding density $0.008 \leqslant \rho_g/\rho_v \leqslant 2.40$ at $1.7 \leqslant \rho_{g\infty}/\rho_{v_s} \leqslant 44.0$, where ρ_{v_s} is the density of saturated vapor at the interface temperature T_s.

The authors of Ref. [91] apparently used for an analysis of condensation from a vapor–gas mixture 'one-component' approximate relations of their own, which are intended to describe the "kinetic boundary conditions at the interface." They came, as a result, to the conclusion that even a small amount of noncondensable gas strongly affects the rate of mass transfer, an observation "of great practical importance, especially for the storage of cryogenic liquids."

Solutions to two problems were presented earlier in [92] in the linearized formulation: recondensation in a flat layer in the presence of a noncondensable gas and condensation–evaporation at the boundary of a semi-infinite volume of a vapor–gas mixture. The moment method was used to solve the model kinetic equation. Formulas have been derived that enable determination of the mass fluxes and concentration fields in the entire range of Knudsen numbers. As a develop-

ment of this approach, it was shown in [93] in considering condensation from a layer of a vapor–gas mixture of thickness d that the kinetic effects near the interface cannot be disregarded if the inequality $1-\gamma(0) \leqslant \mathrm{Kn}$ is fulfilled, where $\gamma = \rho_v/\rho_{mixt}$, $\mathrm{Kn} = l/d$, and l is the mean free path of vapor molecules.

4.3 Experimental data on evaporation–condensation in the presence of a noncondensable component

A description of an experimental study and the corresponding experimental data on the recondensation of naphthalene in the presence of air are presented in [94]. The experimental setup was a sublimation chamber consisting of two spheres, one of which was symmetrically located inside the other. Deposited on the surface of the inner sphere 30 mm in diameter was a naphthalene layer, which sublimated in the course of the experiment. The produced vapor passed through a spherical gap 60 mm thick and deposited on the inner surface of the outer sphere 150 mm in diameter. Heat was supplied to the evaporator, the role of which was played by the inner sphere, by an electric heater located inside the evaporator. The condenser (outer bronze sphere) was cooled by pumping methanol at temperatures from $\approx 0\,^\circ\mathrm{C}$ to $-40\,^\circ\mathrm{C}$ through copper pipes of a heat exchanger wound on the outer surface of the condenser. The mass flux, i.e., the recondensation rate, was measured by the weight method; thermocouples measured the surface temperatures of the sublimator and condenser, which were used to find the corresponding saturation pressures of naphthalene. The total pressure in the chamber was measured using a diaphragm vacuum meter and a U-shaped oil pressure gauge in the range from 10^{-4} to 10^{-1} mm Hg. The sublimator temperature varied in the range of $-21\,^\circ\mathrm{C} - 10\,^\circ\mathrm{C}$, and that of the condenser, from about $-31\,^\circ\mathrm{C}$ to zero. The uncertainties in measuring the temperatures of the inner and outer spheres were $\pm 0.1\,^\circ\mathrm{C}$ and $\pm 0.4\,^\circ\mathrm{C}$, respectively. The error in the measurement of the sublimation flow rate estimated by the authors of [94] is $\pm 2\%$.

The experiments yielded values of the mass flux density (recondensation rate) that ranged from 10^{-5} to 10^{-3} kg m^{-2} s^{-1}. The minimum saturation pressure at the corresponding evaporator temperature (about $-21\,^\circ\mathrm{C}$) was 0.485×10^{-3} mm Hg, the maximum at a temperature of $\approx 10\,^\circ\mathrm{C}$ was 18.200×10^{-3} mm Hg. These values for the condenser were 0.115×10^{-3} mm Hg at $-31\,^\circ\mathrm{C}$ and $\approx 6 \times 10^{-3}$ mm Hg at a temperature $\approx 0\,^\circ\mathrm{C}$. The pressure of the noncondensable component (air) ranged from 1.88×10^{-3} mm Hg to 137.10×10^{-3} mm Hg. Good agreement is noted with the results of calculations that use the diffusion formula for continuous medium conditions and the Hertz–Knudsen formula at a condensation coefficient of 0.9 for the free-molecular limit.

An experimental study of the recondensation of water, freon 113, and mercury in the presence of a natural noncondensable component, air, is reported in [95]. Alumel-chromium thermocouples with a bead about 0.3 mm in size were used in the experiment to measure the temperature distribution in the recondensation gap at an average pressure of 1–2 mm Hg for water and freon 113 and for mercury at a pressure from 0.025 to 0.28 mm Hg. It was found in the experiments that temperature jumps near the interphase surfaces in the process of mercury recondensation may amount to about 50% of the total temperature difference. The authors of [95] came to the conclusion that an important role is played in suchlike phenomena by the presence of a noncondensable component, the presence of which must be quantitatively controlled, and that the most expedient approach in exploring recondensation is the study of monoatomic vapors with a large molar mass at low pressures.

Review [96] contains a formula for determining the mass flux density during evaporation, which was obtained using the methods of quantum mechanical statistical theory [97]. To substantiate this formula, the authors of [96] presented the results of experiments on the evaporation of water near the triple point in a three-dimensional problem in the presence of a noncondensable component, the quantitative content of which was apparently either not recorded by them or not quoted in [96].

5. Problem of formulating boundary conditions

It becomes necessary in studying transfer phenomena to formulate boundary conditions at interphase surfaces that limit the areas under consideration. The so-called quasi-equilibrium scheme [76], which is the simplest version of special consistency conditions, is usually (and rather successfully) used to this end. A well-known example of this kind is the so-called sticking conjecture. The temperatures and velocities of the phases that contact at the interface are as per this hypothesis equal, i.e., neighboring media do not slide relative to each other. However, as the transfer rate increases in the direction normal to the interface, these simple conditions fail to adequately describe the actual picture near the interface. The reason for the resulting misrepresentation of the actual situation is that, in the general case, the transfer process is a nonequilibrium one and, as a consequence, the use of the quasi-equilibrium approach is not substantiated. It becomes relevant in this situation to use the methods of physical kinetics, in which no restrictions are initially imposed on the degree of nonequilibrium of the processes under study. To estimate the degree of nonequilibrium of transfer problems, it is convenient to introduce nonequilibrium parameters, the calculation of which enables determination of whether the quasi-equilibrium scheme or methods of physical kinetics should be used in each specific case.

(1) *The ratio of the flows realized in specific conditions with respect to the maximum possible flow values determined by the MKT.* We consider the effect of a heat flux with a specific quantity q on the surface of the condensed phase. When heat is supplied from the surface of the condensed phase, evaporation begins. The mass flux density of the evaporating substance is denoted as j. It is necessary to determine the relationship between the vapor pressure P'' and the interface temperature T_s and the value of j. As noted in Section 2.2.1, to calculate the mass flux density in the process of evaporation, Eqn (5) may be used, which approximates the results of Ref. [54]. This formula shows that, in general, the vapor pressure during evaporation differs from the equilibrium pressure that corresponds to the temperature of the interface T_s along the saturation line.

We consider as an illustration the following situation. A heat flux $q = 2 \times 10^6$ W m^{-2} is assumed to affect the surface of water with a temperature $T_s = 281$ K. Using the relationship between the heat flux and the specific heat of vaporization $j = q/r$, it is easy to obtain the following value: $j \approx 0.81$ kg m^{-2} s^{-1}. It is assumed in this case that all incoming heat is consumed for evaporation alone. Equation (5) shows that at $T_s = 281$ K ($P_s = 1072$ Pa, $\rho_s = 0.0083$ kg m^{-3}), the mass flux density $j \approx 0.81$ kg m^{-2} s^{-1} is realized at

$\rho_\infty = 0.0048$ kg m^{-3}. The calculation based on method [54] shows that in this case $P_\infty \approx 530$ Pa; the pressure in the vapor at a certain (in the macroscopic sense, rather small) distance from the interface differs by a factor of approximately two from the pressure that corresponds to the temperature of this interface along the saturation line.

For another temperature, namely that of the triple point of water, $T_s = 273.16$ K ($P_s = 611$ Pa) and, thus, $\rho_s = 0.0048$ kg m^{-3}. Consequently, the maximum mass flux density of the molecules j_e that escape from the condensed phase, which is determined by the formula $j_e = \rho_s\sqrt{RT_s/(2\pi)}$, is 0.69 kg m^{-2} s^{-1}. The maximum possible evaporation rate for a stationary setting is approximately 0.80–0.84 of this value (see above), i.e., about 0.56 kg m^{-2} s^{-1}. The maximum heat flux removed as a result due to evaporation is $q = jr = 1.41 \times 10^6$ W m^{-2}. If the heat flux supplied to the phase interface is greater than this value, the excess heat will be spent on heating the condensate, and the temperature of the interface will increase, which in turn will lead to an increase in the evaporation rate. Thus, the relation $q = jr$ will fail due to the capacities of the condensed medium being finite rather than unlimited, as is implicitly assumed in the standard approach. Figuratively speaking, the flow of mass fails to cope with the flow of heat.

It is convenient to introduce in the situation under consideration the following nonequilibrium parameter, which is the ratio of the evaporation rate that corresponds to the incoming heat flux in terms of the vaporization heat and the mass flux density of molecules that escape from the condensed phase:

$$\tilde{j} = \frac{q}{r\rho_s\sqrt{RT_s/(2\pi)}}\,. \tag{49}$$

The heat flux q that actually arrives at the interface may be compared with the heat flux $P_{sat}\sqrt{2RT_s}$ determined by the MKT in the form of the ratio

$$\tilde{q} = \frac{q}{P_{sat}\sqrt{2RT_s}}\,. \tag{50}$$

If the values of $\tilde{j}$ and $\tilde{q}$ are close to or greater than unity, the quasi-equilibrium approach cannot be used, and the MKT methods should be applied.

(2) *The degree of rarefaction of the medium that is characterized by the Knudsen number*. The free-molecular limit, for which the Knudsen number is large, is usually associated with a high or ultrahigh vacuum. However, given the current interest in nanosystems, this regime may also be of importance under normal conditions. Suppose, for example, that the magnitude of the heat flux from one wall of a nanochannel (with temperature T_h) to the other (with temperature T_c) through a flat gas layer 1 nm thick at atmospheric pressure should be calculated. The average free path under normal conditions is $\sim 10^{-7}$ m, consequently, $\mathrm{Kn} \sim 10^{-7}/10^{-9} \gg 1$. This implies that the free-molecular regime is realized in this situation; the use of the standard Fourier law of thermal conductivity is inappropriate, and the following formula should be used to calculate the heat flux at $\Delta T/T_h \ll 1$, where $\Delta T = T_h - T_c$:

$$q = 2\bar{P}\sqrt{\frac{R}{2\pi T_h}}\Delta T. \tag{51}$$

(3) *The ratio of the characteristic times of the corresponding transfer processes*. The necessity of using the MKT methods may be assessed in each specific situation by comparing the time of kinetic relaxation with the characteristic time of the process under consideration:

$$\tilde{\tau} = \frac{\tau_{kin}}{\tau_{proc}}\,. \tag{52}$$

The kinetic relaxation time under normal conditions is $\sim 10^{-9}$ s. Consequently, if the characteristic time of the process is about 10^{-9} s, then $\tilde{\tau} \sim 1$. It is necessary to use in this case the methods of physical kinetics. On the other hand, if the characteristic time of the process is $\sim 10^{-3}$ s, then $\tilde{\tau} \ll 1$, and the methods of continuum mechanics may well be used.

(4) *The ratio of the characteristic pressure drops caused by nonequilibrium effects and specific features of the phenomena under study* (*hydrostatic pressure, pressure difference associated with surface tension, etc.*). For example, in determining the shape of the interface during film boiling on the surface of a heater immersed in a liquid (Fig. 22), the following nonequilibrium parameters may be introduced:

$$\frac{\rho g h_0}{0.44\,q_s/\sqrt{2RT'}}\,, \qquad \frac{2\sigma/R_s}{0.44\,q_s/\sqrt{2RT'}}\,. \tag{53}$$

The hydrostatic pressure and the pressure jump according to the Laplace formula are compared in this case with the pressure difference due to the nonequilibrium heat transfer, which is determined on the basis of the molecular kinetic approach. If the presented parameters are comparable to unity, the methods of physical kinetics should be used.

It seems attractive to use a combined (matched) version of the description. It implies that the liquid phase and the region near the interface are described using molecular dynamics (MD) methods; next, the methods of the kinetic theory of gases are applied; and at a distance exceeding 10–20 free path lengths of gas molecules, CM equations are employed. However, suchlike attempts face certain problems and

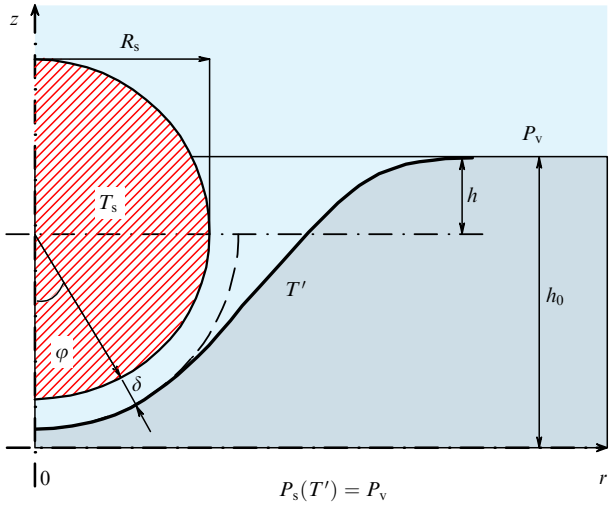

Figure 22. Shape of the interface in film boiling on the surface of a spherical hot body. R_s is the radius of the heated sphere, T_s is its temperature, T' is the temperature of the vapor–liquid interface, $P_s(T')$ is the vapor pressure that corresponds to this temperature along the saturation line, P_v is the vapor pressure over the free surface of the liquid, h is the depth to which the center of the sphere is immersed into the liquid, z and r are the longitudinal and radial coordinates in the spherical reference frame, h_0 is the depth to which the 'zero' point of the spherical reference frame is immersed, φ is the angle between the z axis and the normal to the interface, and δ is the thickness of the vapor film.

difficulties [98]. The characteristic MD time scale is the period of vibrations of the atoms of the crystal lattice, i.e., $\sim 10^{-13}$ s. This value is approximately 10^4 times less than the kinetic relaxation time in vapor under normal conditions, $\sim 10^{-9}$ s. The time step in the numerical implementation of MD is usually $\sim 10^{-14}-10^{-15}$ s. Consequently, to obtain information on the behavior of a system of atoms during the average time of one collision between them, 10^5 steps are needed. Moreover, while in using the matching MKT–CM version there are no conceptual difficulties in the 'exchange' of information, unresolved difficulties emerge in matching MD and MKT. One of them is as follows. The MD simulation methods operate with the coordinates and velocities of the particles of the system under consideration. It is known at the same time that such a description of the gas motion is too detailed in the molecular-kinetic approach. Therefore, a less complete statistical description of the system's behavior should be used. Thus, the molecular kinetic calculations do not enable obtaining the information on the coordinates and velocities of particles necessary for MD. Consequently, the exchange by the results of calculations obtained by molecular kinetic and molecular dynamics simulation methods becomes problematic and, as a consequence, these approaches are difficult to combine.

There are only a few studies wherein the liquid and gas phases are modeled in considering evaporation and condensation on the basis of a single computational method — MD or kinetic equations suitable for describing both rarefied (vapor) and dense (liquid) media. Studies [99–103] may be quoted as examples of such an approach. An original development of this technique was presented at the 31st International Symposium on the Dynamics of Rarefied Gases in report [104], wherein it was proposed to use Grad's moment method to formulate a closed system of 26 moment equations. In the opinion of the authors of [104], "within the appropriate limits, these equations will be reduced to a system of Navier–Stokes–Fourier equations for liquid and vapor. Our primary interest is focused on the study of nonhydrodynamic effects, in particular, transfer through the transition region and interactions of the transition region with the Knudsen layer."

6. Application of molecular dynamics methods

It should be noted that the formulation of the problem for kinetics differs from that for molecular dynamics. The differences are as follows. The condensate–vapor phase interface in the kinetic approximation is a geometric surface, while a transition layer emerges in the MD approach, wherein the properties change quite significantly, but continuously, from the values for condensate to the values for vapor. To carry out kinetic calculations, a condensate-vapor phase equilibrium line (saturation line) should be specified, i.e., dependence of the equilibrium pressure or density of saturated vapor on temperature. Such information, which was obtained experimentally for most substances, is presented in the form of tables, approximating formulas or graphs. This dependence is described by the Clapeyron–Clausius equation (CCE), which allows calculating the derivative of the saturation pressure with respect to temperature $(\mathrm{d}P/\mathrm{d}T)_{\mathrm{sat}}$:

$$\left(\frac{\mathrm{d}P}{\mathrm{d}T}\right)_{\mathrm{sat}} = \frac{r\rho''\rho'}{T(\rho''-\rho')}\,, \tag{54}$$

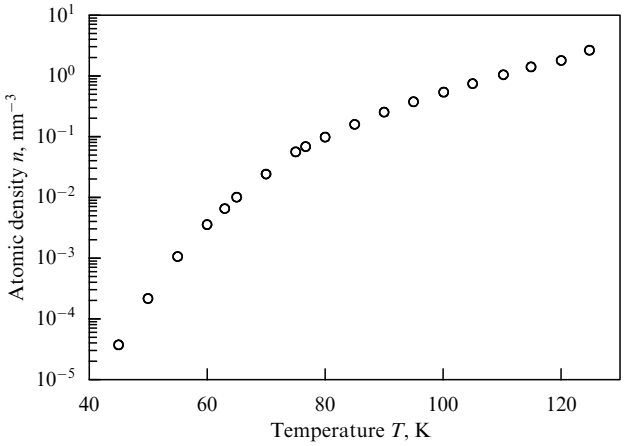

Figure 23. Density of the number of atoms in saturated argon vapors as a function of temperature.

where r is the heat of vaporization, and ρ'' and ρ' are the densities of saturated vapor and liquid, respectively. It is not difficult to find a solution to this equation under the assumption that the vaporization heat is constant for states far from the critical point, when $\rho'' \ll \rho'$ and the Mendeleev–Clapeyron equation is valid:

$$P_{\mathrm{sat}} = \rho'' RT\,, \tag{55}$$

where R is the individual gas constant. The two presented equations yield in this case

$$P_{\mathrm{sat}}(T) = P_{\mathrm{sat}}(T_0)\exp\left[\frac{r}{R}\left(\frac{1}{T_0}-\frac{1}{T}\right)\right], \tag{56}$$

where $P_{\mathrm{sat}}(T_0)$ and $P_{\mathrm{sat}}(T)$ are the saturation pressures at temperature T_0 and T, respectively. Consequently, if the saturation pressure at a certain temperature T_0 and the heat of vaporization r are known, the saturation pressure at any temperature T can be easily calculated.

The MD methods make it possible to avoid empirical determination of the saturation pressure $P_{\mathrm{sat}}(T_0)$ and the heat of vaporization r. It is sufficient to only set the parameters of a potential of interaction between the condensate molecules (atoms), and the saturation line can be obtained by calculating the corresponding equilibrium states, moreover, in the entire temperature range, including near the critical point.

To determine the concentration (density of the number of atoms) of saturated vapor as a function of temperature, a series of MD calculations for argon has been carried out in our studies [105–107], where the MD method was successfully applied to study intense evaporation in vacuum and to solve the recondensation problem. The smoothed Lennard-Jones potential [108] with $\sigma = 0.3426$ nm and a cutoff radius of 0.8125 nm was used for modeling. The results of these calculations obtained in Ref. [107] are displayed in Fig. 23.

The performed calculations of the saturation line of the model argon are a necessary first step, which makes it possible to match the MD and MKT approaches for comparative modeling. Thus, for kinetics, the temperatures of the interphase surfaces and the equilibrium vapor densities corresponding to them along the saturation line are set, while, in molecular dynamics, only the temperatures of condensed phases ('hot' and 'cold' liquids) are specified.

The progress made from the Hertz–Knudsen formula to the solution to rather complex problems, including those for vapor–gas systems, under strongly nonequilibrium conditions has shown that application of the MKT methods is very fruitful. However, to solve the main equation of this theory, the Boltzmann kinetic equation, boundary conditions are needed in the form of the velocity distribution function of molecules that move from the interface. Two flows of molecules are involved in the formation of the DF. One of them is due to directly evaporated molecules, while the other, to reflected ones. A more complex classification is proposed in [109–112]. For example, molecular exchange is also considered in [112], which is understood as a short-term stay of an arriving molecule in a condensed phase, after which this molecule returns to vapor. This implies that in the opinion of the authors of [112] the reflected molecules are those that, without lingering on the surface, immediately move into the vapor phase, while those that have undergone molecular exchange appear there after a relatively short time. It is not very clear what the purpose of such a division is, so we assume further that the evaporated particles are the molecules that come from the bulk of the condensate into the vapor, while the reflected molecules are those that, initially being in vapor, return to it after a stay in the interphase transition layer (interphase). Strictly speaking, such a stay may affect the formation of a flow of evaporating molecules, but for now we ignore this effect, leaving for further research the identification of the conditions under which such an effect may be significant.

To determine the DF of evaporated particles, we consider the movement of atoms from the bulk of the condensed phase to its surface through the interphase layer. Assuming that the condensed phase is at rest, and a flow of evaporated matter flows out of the interphase layer, it should be recognized that a mass flow emerges inside this transition layer. The density gradually decreases, and the flow rate increases in the transition from the condensate to the outer boundary of the interphase layer. The heat flux supplied to the condensate is spent in this case on the formation of the corresponding mass and heat flux in the interfacial layer, the atoms of which acquire a nonzero flux velocity and continue to exchange kinetic energy in collisions with the nearest neighbors. As a result of such interactions, part of the energy flux is used to overcome the attraction of atoms, and the other part, to maintain the thermal energy of the atoms (feeding their kinetic energy). Molecular dynamics simulations [105, 107] show that what occurs is not individual atoms abruptly overcoming a high potential barrier equal to the vaporization energy, but rather a gradual decrease in the effective work function, since the density of atoms near the outer boundary of the transition layer is relatively small and approaches the density of saturated vapor.

The MD simulations show that the DF of atoms in the condensed phase, represented in terms of kinetic energy $\varepsilon_\mathrm{l} = mu_\mathrm{l}^2/2$, where u_l is the component of the velocity of an atom in the liquid normal to the interface, is Maxwellian, i.e., has the form

$$f(u_\mathrm{l})\,\mathrm{d}u_\mathrm{l} = \left(\frac{m}{2\pi k_\mathrm{B}T}\right)^{1/2} \exp\left(-\frac{mu_\mathrm{l}^2}{2k_\mathrm{B}T}\right)\mathrm{d}u_\mathrm{l}\,. \qquad (57)$$

It may be assumed in the naïve mode of evaporation that if an atom that escapes from a fluid had in the fluid average potential energy ε_b and kinetic energy ε_l related to

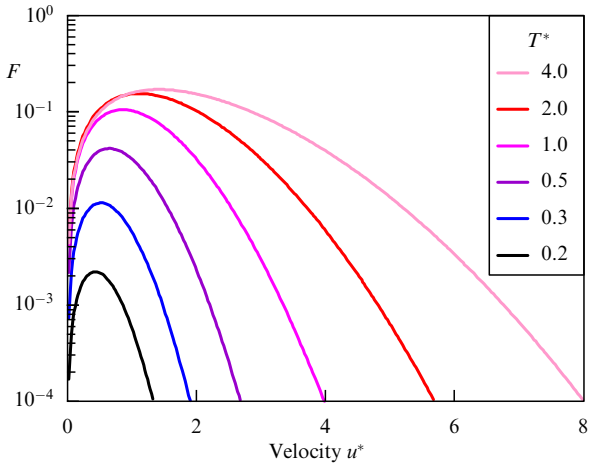

Figure 24. (Color online.) Distribution function F of evaporated atoms for various temperatures of liquid T^* and fixed potential barrier $\varepsilon_\mathrm{b}^* = 1$ in the naïve model of evaporation.

the velocity component directed to the vapor, it would have in the vapor kinetic energy $\varepsilon = \varepsilon_\mathrm{l} - \varepsilon_\mathrm{b}$. Since $\mathrm{d}\varepsilon = mu\,\mathrm{d}u$, $\mathrm{d}\varepsilon_\mathrm{l} = mu_\mathrm{l}\,\mathrm{d}u_\mathrm{l}$, and $\mathrm{d}\varepsilon = \mathrm{d}(\varepsilon_\mathrm{l} - \varepsilon_\mathrm{b}) \equiv \mathrm{d}\varepsilon_\mathrm{l}$, where u is the component of the atom velocity in the vapor normal to the interface, Eqn (57) may be used to derive a formula for the DF of vapor atoms over this velocity $F(u)$. Using the definition $\varepsilon_\mathrm{b} = k_\mathrm{B}T_\mathrm{b}$, we introduce dimensionless quantities $T^* = T/T_\mathrm{b}$, $\varepsilon^* = \varepsilon/(k_\mathrm{B}T_\mathrm{b})$, and $u^{*2}/2 = mu^2/(2k_\mathrm{B}T_\mathrm{b})$. Taking into account that $2f\,\mathrm{d}u_\mathrm{l} = F\mathrm{d}u^*$, we transform the expression for F into

$$F(u^*) = \frac{1}{\sqrt{\pi T^*}} \exp\left(-\frac{u^{*2}/2 + \varepsilon_\mathrm{b}^*}{T^*}\right) \frac{u^*}{\sqrt{u^{*2}/2 + \varepsilon_\mathrm{b}^*}}\,. \qquad (58)$$

Figure 24 displays the distribution functions F calculated for the fixed value of the potential barrier, $\varepsilon_\mathrm{b} = 1$, and various temperatures of liquid. We omit below the $*$ superscript of T^*, ε_b^*, and u^*. The figure shows that the maximum of the DF of evaporated particles is shifted at higher temperatures to higher velocities. This may be explained by the fact that, as the temperature of liquid increases, the energy of motion and, consequently, velocities of the particles increase as well. It can also be seen that an increase in the temperature of the surface results in a growth in the number of particles that escape the surface of the liquid.

Figure 25 displays the distribution functions $F(u)$ calculated for the fixed temperature of liquid $T = 1$ and various heights of the potential barrier ε_b. The black curve corresponds to the function calculated using Eqn (58) for $\varepsilon_\mathrm{b} = 0$. Other curves are obtained for $\varepsilon_\mathrm{b} > 0$.

In analyzing the plots, it can easily be seen that, as the potential barrier increases, the maximum of the velocity DF of molecules shifts to higher velocities. An explanation of this behavior is that a larger kinetic energy is required to overcome a 'higher' potential barrier. It can be seen at the same time that an increase in the barrier height results in a decrease in the number of evaporated particles.

Thus, the main conclusion of the presented analysis of the naïve model of evaporation is that, as the barrier for evaporation tends to zero, the DF for evaporated molecules tends to half-Maxwellian, and the fraction of molecules evaporated in the case of a large potential barrier decreases. We show below that in reality evaporation is not an event by

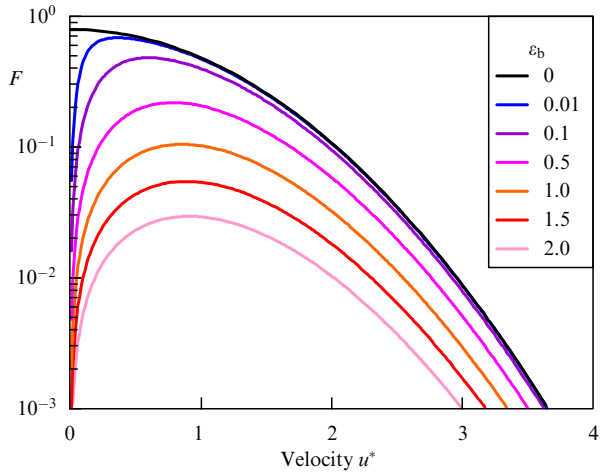

Figure 25. (Color online.) Distribution function F of evaporated atoms as a function of potential barrier height ε_b at the fixed temperature $T = 1$ in the naïve model of evaporation.

which a molecule individually overcomes a barrier, as is assumed in the naïve model, but occurs gradually due to the collective supply of energy by all molecules in the interphase for the movement of individual molecules from the interphase into vapor [107].

It should be noted that the potential barrier that prevents the 'escape' of a molecule from the liquid surface to the vapor region is due to the forces of attraction from the atoms located in the immediate environment of the evaporating molecule. It is well known that the boundary of a liquid is not a clear-cut geometric surface. There is an interphase transition layer from the liquid to vapor whose thickness is several nanometers, wherein the local density of the number of atoms averaged over a sufficiently large area in this layer smoothly decreases from the density of the liquid to that of the vapor. The structure of the interphase was investigated in detail in MD calculations [105, 106], which demonstrated, in particular, the change in the pair correlation function of the distribution of atoms in the transition from liquid to vapor and showed that due to capillary waves the correlation radius in the interphase significantly exceeds that in liquid.

MD simulation [107] of the stationary regime of evaporation of argon atoms from the surface of a liquid at $T = 80.4$ K and condensation onto a cold surface at $T = 72.4$ K yields the coordinate dependences of the density of the number of argon atoms and the average potential energy of atoms in the vicinity of the transition layer between the evaporating liquid and the outgoing vapor, which are shown in Fig. 26a. The numbered gray stripes indicate the position of thin layers (with a thickness of about 0.26 nm) parallel to the interphase in which the planar sections of the pair correlation functions $n_2(\mathbf{r}_1, \mathbf{r}_2)$ were calculated. Due to the symmetry of the liquid–vapor system with a planar interphase, these sections are radial functions of the distribution of pairs of atoms $n_2(r; x)$ over the interatomic distance $r = (x_{12}^2 + y_{12}^2 + z_{12}^2)^{1/2}$, which have close coordinates, $|x_{12}| = |x_1 - x_2| < 0.05$ nm, on the evaporation axis. The radial functions $n_2(r; x)$ displayed in Fig. 26b tend to the function $n(x)$, $n_2(r; x) \to n(x)$, at $r \to \infty$, where $n(x)$ is the average density of the number of atoms in a thin layer with coordinate x. It is clearly seen that, as the interphase is passed through, the distant coordination peaks in $n_2(r)$ vanish, and long falling 'tails' emerge in the distribution functions. These tails are determined by long-range correlations of density fluctuations in the transition layer, which arise due to thermally excited capillary waves [106, 113].

It is of importance to note the following phenomenon found in MD simulation [107]. The density changes significantly in the transition layer, while the temperature remains approximately equal to that of the liquid in most of the interphase. This can be seen in the coordinate dependences of the density of the number of argon atoms and temperature in the vicinity of the transition layer displayed in Fig. 27. The observed drop in temperature only occurs at the very interface of the interphase with the vapor phase, where the average potential energy of atoms, and, consequently, their barrier for evaporation has already significantly approached zero.

The presented calculations show that the transition from liquid to vapor occurs not through a sharp transformation (instant loss of phase transition energy by particles of liquid), as a result of which the heat of evaporation is consumed, but due to the gradual, on the MD scale, consumption of energy of the interphase medium for the advancement of the atom from the bulk of the condensate outward. It should be noted that the probability of evaporation (i.e., transition from the domain of liquid to the domain of vapor) of particles located in the regions of the transition layer closest to the vapor is greater than that for particles located in the 'deeper' regions of the transition layer. Moreover, the potential barrier, which

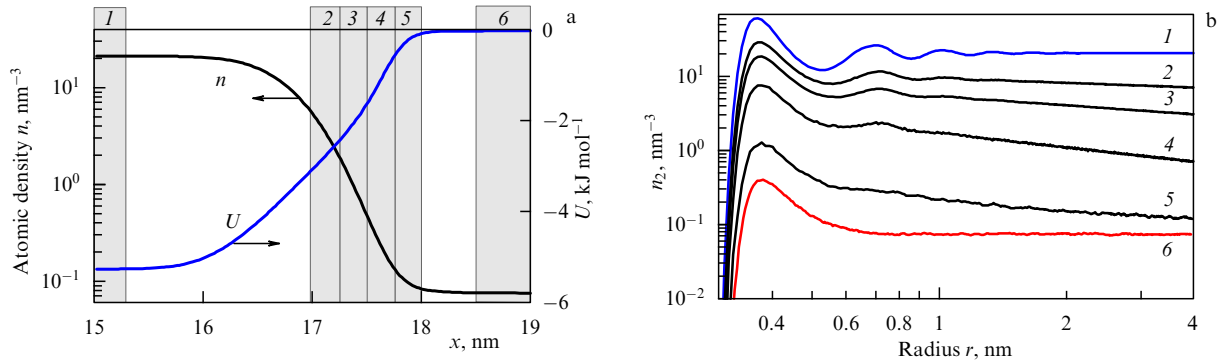

Figure 26. (Color online.) (a) Change in the average density of the number of atoms $n(x)$ and the average potential energy of argon atoms $U(x)$ in a planar liquid–vapor transition layer during evaporation of liquid argon at $T = 80.4$ K. Numbered gray stripes indicate the position and thickness of the layers in which the radial distribution functions of atoms $n_2(r; x)$ were calculated. (b) Change in $n_2(r; x)$ for pairs of atoms with close coordinates, $|x_{12}| < 0.05$ nm, located in the numbered layers parallel to the interphase. The function $n_2(r; x)$ coincides in the bulk phase of liquid (blue curve) and vapor (red curve) with the conventional spherical radial DF $n_2(r)$.

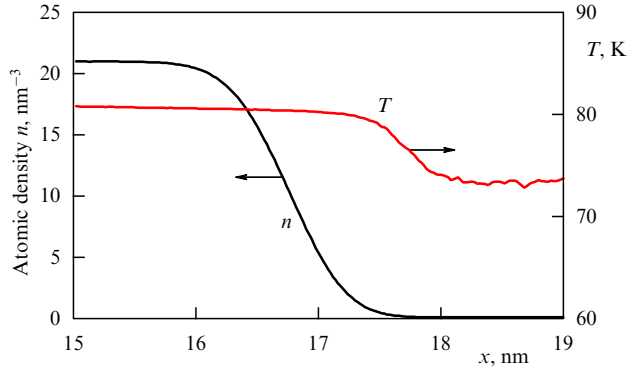

Figure 27. Change in the average density of the number of atoms $n(x)$ and temperature $T(x)$ in a planar transition liquid–vapor layer in the process of condensation from the surface of liquid argon at $T = 80.4$ K.

these particles must overcome, approaches zero, and the temperature of the 'escape region' is close to the temperature of the liquid. It should be emphasized that temperature of the liquid is maintained constant in the considered version of the calculation; therefore, the loss of energy of the phase transition as a result of movement from deep layers of the liquid to the outer boundary of the transition layer is compensated by the constant supply of heat to the evaporating atoms.

In approaching the outer boundary of the interphase, the behavior of an ensemble of molecules becomes increasingly similar to that of vapor molecules, which means that the attractive forces and the average potential energy of molecules decrease, and their average kinetic energy barely changes due to intermolecular collisions during which energy can be transferred to particles in the interphase from deeper particles. Thus, the effect of the attraction forces that determine the work function decreases in passing to the outer boundary of the interphase, while the effect of collisions, i.e., the repulsion branch, increases. As a result, nothing slows down a moving atom (molecule) on the external boundary, and it escapes into the vapor, virtually without spending its own kinetic energy on this transition.

An approach was proposed in [107] for a more thorough derivation of the distribution function of evaporated molecules. It is noted that evaporation is always accompanied by the condensation of evaporated atoms, which gain a reverse velocity due to interatomic collisions in the outgoing vapor. The probability of such collisions that throw the molecules back to the interface increases as the vapor region expands. To eliminate the backflow generated by the collisions, an absolutely cryogenic surface was placed near the interface during the simulation, which adsorbed the molecules incident on it. This technique enabled determination of a flux of evaporated atoms and the corresponding distribution function not distorted by collisions with atoms that move from the bulk of the vapor region to the interphase. The results obtained (for the recondensation problem) are shown in Fig. 28a.

The interphase region (interphase) may be divided into two almost equal parts. The first of them is the inner part between the bulk (deep) phase and the cross section, on which the temperature profile is separated into longitudinal T_x and transverse T_y. The left boundary of the nonequilibrium part of the interphase layer (left vertical dashed line) is determined by the point where the longitudinal, T_x, and transverse, T_y, temperatures diverge. This point is used to determine the

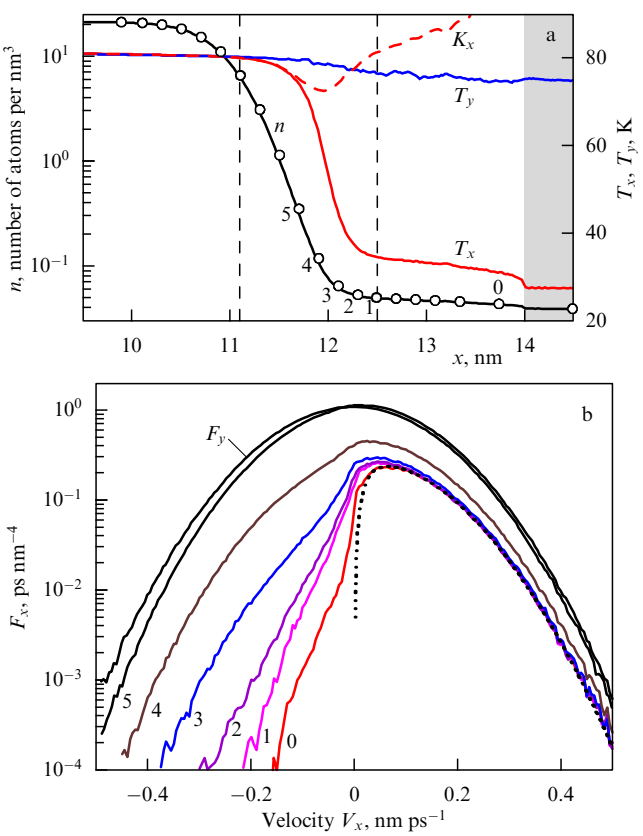

Figure 28. (Color online.) (a) Profiles of atomic density and temperature near the hot interphase in the vapor region 1.5 nm thick limited by a cryogenic layer at $x > 14$ nm. Kinetic energy K_x is measured in units of temperature. The dots on the density profile indicate the positions and numbers of the thin layers in which the DFs are calculated. (b) Evolution of the distribution function F_x for the longitudinal component of the velocity V_x measured in several thin layers within the nonequilibrium part of the interphase layer. The numbers on the curves correspond to the numbers of the layers indicated in Fig. a. The last DF near the interphase boundary has number 1, and the DF in the vapor is number 0. The thin black curve shows the DF for the transverse component of the velocity V_y. The dashed curve corresponds to the DF obtained in the naïve model of evaporation for the barrier equal to 0.0032 of the binding energy of atoms in the liquid.

surface temperature T_h. The right boundary (right dashed line) corresponds to the point at which the density and T_x begin to decrease in a linear way. Maxwell's demon ensures the fulfillment of the inequality $V_x > 0$ for atoms in the gray-shaded zone. The atoms pass through the interphase almost without losing their longitudinal component of the kinetic energy K_x. The temperature equilibrium in the inner part of the interphase is well maintained, since the drift velocity is low, and a sufficiently long time (more than 200 ps) is needed to cross this part.

As the density decreases by a factor of 3.5 at the end of the inner equilibrium part, the temperature T_x begins to decrease, and the drift velocity increases, attaining a value of more than 5 m s^{-1}. This coordinate may be considered the beginning of the second nonequilibrium part of the interphase, within which the flow velocity increases to 100 m s^{-1} at the coordinate shown by the right straight dashed line in Fig. 28a. The drift time is reduced in this case to 20 ps, a value which is comparable to the collision time. This leads to significant changes in the shape of the DF, which occurs between approximately the middle of the interphase and its

right boundary, namely, between points 5 and 1 shown in Fig. 28a.

Figure 28b illustrates the changes in the DF obtained by MD simulation within 1.2 ns after steady-state evaporation regime has been attained. It can be seen that the main changes in the DF occur in the interphase layer; the fraction of the DF with negative velocities decreases and its width greatly decreases as well when approaching the right edge of the interphase, while the width of the DF for positively directed particles remains almost unchanged. As a result of this evolution, the temperature T_x sharply decreases, but the average kinetic energy of the evaporated atoms K_x changes insignificantly, which can be seen in Fig. 28a. Thus, the formation of the DF of the vapor immediately behind the interphase looks like the evaporation of individual atoms without the loss of their kinetic energy to overcome the potential barrier, as is the case in the naïve model of evaporation, since the barrier should be assumed to be close to zero (see the dashed DF in Fig. 28b).

The results displayed in Fig. 28 show that the DFs of evaporated atoms at the outer boundary of the interphase (curve 1 in Fig. 28b) and in the vapor immediately beyond this boundary (curve 0 in Fig. 28b) are close to the half-Maxwellian for positive normal components of the velocities V_x. The problem of recondensation for argon was investigated in Ref. [107] taking this observation into account by two methods: MD simulation and solution to BKE. The vapor layer was limited on the one side by 'hot' condensate at T_h, and on the other side, by 'cold' condensate at T_c. Two settings were considered: in one of them, $T_h = 80.4$ K, $T_c = 72.4$ K, in the other, $T_h = 79.4$ K, $T_c = 60.5$ K. The thickness of the vapor layer was in both cases such that the Knudsen number was 0.021. The average free path was determined using T_h. The BKE was solved for the settings described above using the method reported in [82]. The distribution functions for atoms that escape from hot and cold condensates were taken in the half-Maxwellian form with a zero transfer rate, based on the MD results considered above. These DFs were used as boundary conditions required for the BKE. The BKE solutions obtained for various values of the evaporation and condensation coefficients were compared with the MD simulation data. This comparison showed that the best agreement between the MD results and BKE solutions is achieved if evaporation and condensation coefficients are close to unity.

Thus, the assertion that evaporation occurs according to a diffuse scheme with an evaporation coefficient equal to unity, and the corresponding DF has a form close to a half-Maxwellian with a zero transfer rate, may be considered to be sufficiently substantiated.

Several studies in which the DF of evaporated molecules had been determined were reported at the 31st International Symposium on the Dynamics of Rarefied Gases held in 2018. For example, a theoretical study of the evaporation of one-component liquids into a vacuum was presented in report [114]. The authors formulate the conclusion of their study as follows: ''Preliminary results based on the numerical solution of the Enskog–Vlasov equation show that no matter how low the temperature is, the distribution function of evaporated atoms is approximated by the anisotropic Maxwellian with different temperatures for the normal interface and the velocity components parallel to it. This anisotropy diminishes with decreasing temperature.'' It is also noted that the average temperature of this Maxwellian is close to the temperature at which the separation of the longitudinal and transverse temperatures of the liquid occurs. Reported in [115] was the intention to measure the DF of water molecules evaporated from the surface of a water droplet with a diameter of 5–10 μm fixed on the end cut of a glass capillary tube. The authors justify the setup they propose by the fact that, in their opinion, the velocity DF of molecules near the interface cannot be represented by the results of measurements using a sensor located at a certain distance from the evaporation surface, as was done in previous experiments by various researchers. This conclusion is based on the conjecture that significant changes in the DF may occur in the process of the collision of molecules on the way from the evaporation surface to the sensor.

Transfer processes near the interface were recently studied in [116] using the MKT and MD methods. The authors solve the model kinetic equation by the moment method, taking the four-moment ellipsoidal distribution as an approximation of the DF of vapor molecules, and came as a result to a conclusion regarding the existence of the above-mentioned anisotropy of vapor temperature in the region occupied by the evaporated particles. An MD simulation with 500,000 argon atoms was performed using the Verlet algorithm. To carry out kinetic calculations, the coefficients of evaporation and condensation were set, and it was assumed that in this case they are equal to each other. It should be noted that the solution of the BKE by the moment method for Maxwellian molecules based on the same approximation was obtained in the problem of intense evaporation by one of the authors of this review (A P Kryukov) and published in [54].

Evaporation in nanoporous membranes was explored in [117, 118]. In the first of these studies, the authors successfully applied in 2015 approach [54] to describe evaporation from nanostructures. In the second publication, at the stage of testing the method of direct statistical modeling used by the authors to calculate evaporation, the data they obtained were compared with the corresponding calculations made using Eqn (5) in Section 2.2. Good agreement was found between the results obtained by these two methods.

In general, determination of the DF for reflected atoms is a more challenging task.

The following three-level hierarchy is proposed.

1. The best approach would be to solve the transfer problems at the interface using the MD methods in the entire macroscopic domain. This is, however, impossible for both technical and, apparently, conceptual reasons. Given the involved time and material costs, it is most likely not necessary, since the 'noise' of the extensive information obtained may be so great that it turns out to be comparable in order of magnitude to the values determined in the macroscopic region.

2. MD is used to determine the DF of particles (molecules or atoms) that move from the interface, i.e., evaporated and reflected particles. This DF is used as a boundary condition in solving the BKE, which is matched with the CM equations. Study [107] shows that the DF of evaporating atoms is half-Maxwellian on both 'hot' and 'cold' surfaces, and the condensation coefficients on both these surfaces are close to unity. Thus, the boundary conditions for the solution of the BKE are formulated. If an artificial (auxiliary) recondensation problem is set for another specific problem in which a 'cold' surface is located, for example, at a distance of 20 free path lengths (or Maxwell's demon is placed at the same or a smaller distance), its solution using MD methods will yield

the DF both near the interface and at a distance of 10 free path lengths. If the DF near the interface is known, it is possible to solve the BKE. If a distribution function is found as a result that coincides with the DF found by the MD method at a distance of 10 free paths (distribution functions are obtained that coincide with the DFs found by the MD method at a distance from 0 to 10 mean free paths), the solution to the general problem is found. If there is no such coincidence, then a new recondensation problem is set with new parameters of an artificial 'cold' surface. The DF is again found near the 'evaporating' boundary and at a distance of 10 free paths from it. Then, the BKE is again solved with the boundary condition in the form of a DF determined by the MD method near the 'evaporating' boundary. As a result of solving the BKE, the DF, which is determined at a distance of 10 free path lengths from the 'evaporating' boundary, is compared with the DF determined by MD methods at this distance. When the MD DF coincides with the BKE DF, the iterative process ends. This agreement must be attained at every step of the BKE solution.

An approximate end-to-end method, either in modification [103] or involving the determination of the condensation coefficient by the MD method as in the version of [119, 120], seems promising from the point of view of applications.

An approximation is conceivable in which the positively directed flow (the sum of the reflected and evaporated flows) is assumed to be independent of the negatively directed flow (that enters the surface). The full MD method is used then up to the first 'kinetic' step to find the distribution function of positively directed molecules (direct DF). Next, it is used as a boundary condition at each kinetic step, at both the first and subsequent steps. The less intense the process under study is, the more justified such a simplification is, since reasons emerge to believe that the DF of negatively directed molecules (reverse DF) changes insignificantly during the evolution of the flow over the entire solution interval. The described simplification may be considered justified even in the case of high rate evaporation, since several researchers have shown that the form of the inverse DF for strong evaporation regimes weakly affects the solutions, inasmuch as this function itself is smaller, and in the limiting situation even much smaller, than the DF of atoms that move in a positive direction (from the interface). Since at present it may be considered confirmed that the DF of evaporated atoms is half-Maxwellian with the temperature of the interface and the corresponding density along the saturation line [107], the main part of the DF for positively directed particles is known. Consequently, a relatively small addition to the DF of positively directed particles from possibly reflected atoms, which is found using MD methods, is unlikely to undergo significant changes during the entire time of the evaporation under study. Thus, it is now sufficient to determine the DF of positively directed molecules only once for the first 'kinetic' step.

The situation is more complicated in the case of strong condensation, where the reverse and direct distribution functions are comparable, and, for supersonic flows, one of them can be much larger than the other. However, if it is necessary to investigate a flow that is stationary on the CM scale in the case of strong condensation, it is proposed to first obtain a BKE solution with a half-Maxwellian for evaporated atoms, the specified (in a relatively arbitrary way) condensation coefficient, and the diffuse character of evaporation as boundary conditions. The results obtained are used further for MD simulation and determination of the DF and, consequently, the condensation coefficient. If the last of these coincides with the value specified at the kinetic stage, the solution is found. Otherwise, a new value of the condensation coefficient is set, and the procedure to solve the BKE and MD modeling is repeated. This iteration is repeated until coincidence occurs. The approach described above is apparently also suitable for nonstationary problems on the CM scale, since the steps on the CM scale are an alternation of the results that are stationary on the kinetic scale.

Difficulties will arise in solving problems of strong condensation on a kinetic time scale.

3. If item 2 cannot be implemented due to its complexity and excessively large number of calculations (in particular, in the problems of strong condensation mentioned in item 2), the following approximate approach is proposed. The limiting value of the condensation coefficient β_{lim} is calculated, and the BKE is solved next for the diffuse nature of the reflection for $\beta = 1$ and for β_{lim}. Conceptually feasible solutions are obtained in this way, and the effect of the condensation coefficient on the solution of a specific problem is determined.

7. Conclusions

Evaporation–condensation problems can be described, in principle, at three levels: within the mechanics of continuous media, using methods of molecular-kinetic theory, and with molecular-dynamic modeling. Each of these approaches has its own advantages, disadvantages, and limitations.

The advantage of CM methods is the deep and multifaceted development of both analytical and numerical methods for solving corresponding equations (usually Navier–Stokes) adapted for research and engineering practice. The list of disadvantages includes the limited degree of nonequilibrium of transfer processes due to assumptions that underlie the derivation of the CM equations and the conceptual unfeasibility of providing a correct formulation of the boundary conditions for problems with permeable interphase surfaces.

The advantages of the MKT are the absence of restrictions on the degree of nonequilibrium of the processes under study, the need to use empirical data much smaller than in the CM (only at the level of the interaction potentials of atoms and molecules), and the feasibility of formulating boundary conditions for problems with permeable interfacial surfaces, this being possible owing to the adaptation of the formulation of problems for the Boltzmann kinetic equation in the language of the molecular velocity distribution function. The disadvantages are the complexity of the BKE that results in the need for high computer performance and large memory and the above-mentioned approach to formulating boundary conditions, which requires the DF for the molecules which escape from condensed media to be known. This DF is usually specified using various models (diffuse or mirror reflection scheme, etc.); less often it is found experimentally and by setting the condensation coefficient.

The condensation coefficient introduced as early as the beginning of the 20th century has apparently exhausted its productive potential, since it depends on a large number of factors and setups, i.e., is not a coefficient, but rather a complex function of many arguments, which does not simplify, but, on the contrary, complicates the solution to the corresponding problems. Several interesting reports on evaporation and condensation coefficients were presented at

the 31st International Symposium on the Dynamics of Rarefied Gases held in 2018. The sound resonance phenomenon was used in [121] to experimentally show that the water evaporation coefficient is close to unity in the temperature range from 295 K to 313 K. An analysis of study [122] presented in report [123] shows that agreement with experiment can only be achieved at a value of the condensation coefficient equal to 0.05. It should be noted that it is the direct experimental determination of the condensation coefficient which is of extreme importance, since it allows proposed calculation models to be confirmed or refuted. Direct experiment is understood as the direct determination of the flux of particles arriving at (incident on) the interface surface at a distance as close to this surface as possible and the similar direct determination of the flux of reflected atoms or molecules.

The advantages of MD are the absence of restrictions on the degree of nonequilibrium of the processes under study, as in the MKT, the need for empirical data only at the level of the interaction potentials of atoms and molecules, and the absence of the need to formulate boundary conditions at the interphase surfaces. Disadvantages are very large computer times required and, as a result, solutions that can only be found for times that do not exceed a few nanoseconds. Progress in the development of computer technology raises hope that this time interval will gradually increase, but the conceptual feasibility of performing classical MD simulation of a system of an acceptable size for an interval of several microseconds seems doubtful, even in the next decade.

One of the most important and urgent tasks is to combine these three approaches to solve actual problems, or at least to suggest ways to implement such a combination.

The experience of 'matching' shows that this procedure is feasible if the solutions of the CM equations and the basic equation of the MKT, the Boltzmann kinetic equation, are conjugated. However, attempts to 'match' MD and MKT failed, and it seems at present that this goal may not be attained.

Prospects may be viewed in at least two directions, which may enrich each other in the process of their development. The first is the creation of a bank of solutions to transfer problems obtained by MD methods for various substances, temperatures, conditions of energy effects, and geometric dimensions. The second avenue is the development of approximate approaches for engineering practice, including those based on the MD results [120, 124]. The use of the Vlasov–Enskog equation for the study of interphase energy and mass transfer in various vapor–liquid systems also deserves special attention.

Study of recondensation problems shows that at known temperatures of 'hot' and 'cold' condensates the mass flux density can be determined with good accuracy using the Hertz–Knudsen formula, even for the limit of a continuous medium. However, this conclusion has become clear only now, almost after 70 years M Plesset [2] published his study, time which was spent obtaining solutions to this problem by various methods of solving the BKE and its models in a wide range of the Knudsen number. The importance of this finding is somewhat devaluated by the observation that the problem of recondensation is more of a model nature rather than a real one, since most of the processes of evaporation and condensation implemented in practice occur in a space that is semi-infinite on the scale of the mean free path of vapor molecules.

Problems with mixtures, even if they only contain two components (vapor and gas), are much more complicated than single-component ones. First and foremost, it is necessary to solve two kinetic equations rather than one, and, as a result, four collision integrals emerge instead of one. Determination of the limiting values of the initial parameters as in Ref. [87] seems to be of use in this situation.

Some interesting features of the behavior of the temperature of evaporating water droplets have been discovered during the study of their vaporization into the air [125]. It has been experimentally observed that the temperature of drops increases at the final stage of their existence. However, a calculation based on the standard approach, wherein the mass transfer rate is computed exclusively from the diffusion equation, and therefore the density of water vapor near the surface of a drop is found as the equilibrium vapor density that corresponds to the temperature of this surface along the saturation line, fails to predict such behavior. Even so, if the kinetics, i.e., the Knudsen layer, are taken into account, qualitative agreement with experiment may be obtained even for relatively crude kinetic models. The effect of kinetic features in studying droplet evaporation into a vapor–gas medium was noted both at a relatively early stage of the study and in the recent past, but such a nontrivial behavior of temperature has only been noticed quite recently. The application of the MKT methods to the study of processes at the interphase surfaces of helium II enabled a number of interesting conclusions to be drawn, some of which are successfully confirmed by experiments.

Acknowledgments. This study was supported by the Russian Foundation for Basic Research (project no. 20-08-00342). The interpretation of experimental data on the transfer processes on the helium II interface was carried out by A P Kryukov with support from the Russian Science Foundation (project no. 19-19-00321).

References

1. Hertz H *Ann. Physik* **253** 177 (1882)
2. Plesset M S *J. Chem. Phys.* **20** 790 (1952)
3. Knudsen M *Ann. Physik* **352** 697 (1915)
4. Marek R, Straub J *Int. J. Heat Mass Transfer* **44** 39 (2001)
5. Risch R *Helv. Phys. Acta* **6** 128 (1933)
6. Crout P D *J. Math. Phys.* **15** 1 (1936)
7. Schrage R W *A Theoretical Study of Interphase Mass Transfer* (New York: Columbia Univ. Press, 1953)
8. Kucherov R Ya, Rikenglaz L E *Sov. Phys. JETP* **10** 88 (1960); *Zh. Eksp. Teor. Fiz.* **37** 125 (1959)
9. Kucherov R Ya, Rikenglaz L E *Dokl. Akad. Nauk SSSR* **133** 1130 (1960)
10. Muratova T M, Labuntsov D A *Teplofiz. Vys. Temp.* **7** 959 (1969)
11. Labuntsov D A *Teplofiz. Vys. Temp.* **5** 579 (1967)
12. Kogan M N *Rarefied Gas Dynamics* (New York: Plenum Press, 1969); Translated from Russian: *Dinamika Razrezhennogo Gaza: Kineticheskaya Teoriya* (Moscow: Nauka, 1967)
13. Pao Y *Phys. Fluids* **14** 306 (1971)
14. Pao Y *Phys. Fluids* **14** 2285 (1971)
15. Shankar P N, Marble F E *Phys. Fluids* **14** 510 (1971)
16. Cipolla J W (Jr.), Lang H, Loyalka S K *J. Chem. Phys.* **61** 69 (1974)
17. Sone Y, Onishi Y *J. Phys. Soc. Jpn.* **35** 1773 (1973)
18. Sone Y, Onishi Y *J. Phys. Soc. Jpn.* **44** 1981 (1978)
19. Thomas J R (Jr.), Chang T S, Siewert C E *Phys. Rev. Lett.* **33** 680 (1974)
20. Koffman L D, Plesset M S, Lees L *Phys. Fluids* **27** 876 (1984)
21. Ytrehus T, Aukrust T, in *Proc. of the 15th Intern. Symp. on Rarefied Gas Dynamics, June 16–20, 1986, Grado, Italy* Vol. 2 (Ed. V Boffi, C Cercignani) (Stuttgart: B.G. Teubner, 1986) p. 271

22. Chernyak V *J. Aerosol Sci.* **26** 873 (1995)
23. Anisimov S I *Sov. Phys. JETP* **27** 182 (1968); *Zh. Eksp. Teor. Fiz.* **54** 339 (1968)
24. Anisimov S I et al. "Action of high-power radiation of metals", NJPRS 53241 (Alexandria, VA: National Technical Informations Service, 1971)
25. Kogan M N, Makashev N K *Fluid Dyn.* **6** 913 (1971)
26. Cheremisin F G *Fluid Dyn.* **7** 351 (1972)
27. Makashev M K *Fluid Dyn.* **7** 815 (1972)
28. Anisimov S I, Rakhmatulina A Kh *Sov. Phys. JETP* **37** 441 (1973); *Zh. Eksp. Teor. Fiz.* **64** 869 (1973)
29. Yen S M *Comput. Fluids* **1** 367 (1973)
30. Anisimov S I, Luk'yanchuk B S *Phys. Usp.* **45** 293 (2002); *Usp. Fiz. Nauk* **172** 301 (2002)
31. Murakami M, Oshima K, in *Proc. of the 9th Intern. Symp. on Rarefied Gas Dynamics, Gottingen, 1974* (Eds M Becker, M Fiebig) (Porz-Wahu: DFVLR-Press, 1974) p. F6
32. Fischer J *Phys. Fluids* **19** 1305 (1976)
33. Ytrehus T, in *Proc. of the 10th Intern. Symp. on Rarefied Gas Dynamics* (Ed. J Potter) (New York: AIAA, 1977) p. 1197
34. Labuntsov D A, Kryukov A P *Teploenergetika* (4) 8 (1977)
35. Bishaev A M, Rykov V A *USSR Comput. Math. Math. Phys.* **18** (3) 182 (1978); *Zh. Vychisl. Matem. Matem. Fiz.* **18** 709 (1978)
36. Knight C J *AIAA J.* **17** 519 (1979)
37. Cercignani C, in *Proc. of the 12th Intern. Symp. on Rarefied Gas Dynamics* (Ed. S Fisher) (New York: AIAA, 1981) p. 305
38. Abramov A A, Kogan M N, Makashev N K *Fluid Dyn.* **16** 381 (1981)
39. Aoki K, Cercignani C *Phys. Fluids* **26** 1163 (1983)
40. Kryukov A P *Fluid Dyn.* **20** 487 (1985)
41. Cercignani C, Fiszdon W, Frezzotti A *Phys. Fluids* **28** 3237 (1985)
42. Hermans L J F, Beenakker J J M *Phys. Fluids* **29** 4231 (1986)
43. Frezzotti A, in *Proc. of the 15th Intern. Symp. on Rarefied Gas Dynamics* (Ed. V Boffi, C Cercignani) (Stuttgart: B.G. Teubner, 1986) p. 313
44. Kryukov A P *Fluid Dyn.* **23** 320 (1988)
45. Abramov A A, Kogan M N *Dokl. Math.* **35** (1) 1 (1990); *Dokl. Akad. Nauk SSSR* **310** 43 (1990)
46. Aoki K, Sone Y, Yamada T *Phys. Fluids A* **2** 1867 (1990)
47. Kryukov A, in *Proc. of the 17th Intern. Symp. on Rarefied Gas Dynamics, July 8–14, 1990, Aachen, Germany* (Ed. A E Beylich) (New York: Wiley VCH, 1991) p. 1278
48. Sibold D, Urbassek H M *Phys. Fluids A* **3** 870 (1991)
49. Sugimoto H, Sone Y *Phys. Fluids A* **4** 419 (1992)
50. Sone Y, Sugimoto H *Phys. Fluids A* **5** 1491 (1993)
51. Ytrehus T, Østmo S *Int. J. Multiphase Flow* **22** 133 (1996)
52. Takata S, Aoki K *Phys. Fluids* **11** 2743 (1999)
53. Sone Y, Sugimoto H, Aoki K *Phys. Fluids* **11** 476 (1999)
54. Labuntsov D A, Kryukov A P *Int. J. Heat Mass Transfer* **22** 989 (1979)
55. Kryukov A P *Protsessy Perenosa v Sushchestvenno Neravnovesnykh Sistemakh* (Transfer Processes in Strongly Nonequilibrium Systems) (Moscow: Izd. MEI, 2013)
56. Niknejad J, Rose J W *Proc. R. Soc. Lond. A* **378** 305 (1981)
57. Ishiguro R, Sugiyama K, Terayama Y, in *Proc. Intern. Symp. on Heat Transfer* (China: Tsinghua Univ. Press, 1985) p. 463
58. Kosasie A K, Rose J W, in *Proc. of the 7th ASME National Heat Transfer Conference, San Diego, California, August 9–12, 1992* (New York: American Society of Mechanical Engineers, 1992)
59. Kryukov A, Sachkova T, in *Condensation and Condenser Design: Proc. of the Engineering Foundation Conf. on Condensation and Condenser Design, St. Augustine, Florida, March 7–12, 1993* (Eds J Taborek, J Rose, I Tanasawa) (New York: ASME, 1993) p. 581
60. Mager R, Adomeit G, Wortberg G, in *Proc. of the 15th Intern. Symp. on Rarefied Gas Dynamics* (Eds V Boffi, C Cercignani) (Stuttgart: B.G. Teubner, 1986) p. 262
61. Schilder R, Adomeit G, Wortberg G, in *Proc. of the 13th Intern. Symp. on Rarefied Gas Dynamics* (Eds O M Belotserkovskii et al.) (New York: Plenum Press, 1985) p. 577
62. Mlynskii A V, Kryukov A P, in *Tr. X Vsesoyuzn. Konf. po Dinamike Razrezhennykh Gazov, 27–30 Iyunya 1989 g.* (Proc. of the 10th All-Union Conf. on Rarefied Gas Dynamics, June 27–30, 1989) Vol. 3 (Moscow: MEI, 1991) p. 144
63. Chepel' S L, Mlynskii A V, Kryukov A P, in *Tr. IX Vsesoyuzn. Konf. po Dinamike Razrezhennykh Gazov, Sverdlovsk, Iyun' 1987 g.* (Proc. of the 9th All-Union Conf. on Rarefied Gas Dynamics, Sverdlovsk, June, 1987) Vol. 2 (Sverdlovsk: Izd. Ural. Univ., 1988) p. 154
64. Aristov V V, Kryukov A P, Cheremisin F G, Shishkova I N *USSR Comput. Math. Math. Phys.* **31** 111 (1991); *Zh. Vychisl. Matem. Matem. Fiz.* **31** 1093 (1991)
65. Mayer E et al., in *Proc. of the 4th Intern. Symp. on Rarefied Gas Dynamics* (Toronto: Academic Press, 1966) p. 239
66. Furukawa T, Murakami M, in *Proc. of the 21st Intern. Symp. on Rarefied Gas Dynamics, 26–31 July, 1998, Marseille, France* Vol. 1 (Eds R Brun et al.) (Toulouse: Cépadues-Ed., 1999) p. 519
67. Maki M, Furukawa T, Murakami M, in *Book of Abstracts of the 22nd Intern. Symp. on Rarefied Gas Dynamics, Sydney, Australia, 9–14 July 2000* (Eds T J Bartel, M A Gallis) (New York: AIP, 2000)
68. Kryukov A P, Levashov V Yu *Int. J. Heat Mass Transfer* **54** 3042 (2011)
69. Wiechert H, Buchholz F, in *Liquid and Solid Helium, Proc. EPS Topical Conf. Haifa* (Eds C G Kuper, S G Lipson, M Revzen) (New York: Wiley, 1975) p. 293
70. Kryukov A P *Elementy Fizicheskoi Kinetiki* (Physical Kinetics: a Primer) (Moscow: Izd. MEI, 1995)
71. Labuntsov D A, Kryukov A P *High Temp.* **25** 404 (1987); *Teplofiz. Vys. Temp.* **25** 536 (1987)
72. Kryukov A P, Van Sciver S W *Cryogenics* **21** 525 (1981)
73. Gorter C J, Mellink J H *Physica* **15** 285 (1949)
74. Kryukov A P, Mednikov A F *J. Appl. Mech. Tech. Phys.* **47** 836 (2006); *Prikl. Mekh. Tekh. Fiz.* **47** (6) 78 (2006)
75. Haefer R A *Kryo-Vakuumtechnik. Grundlagen und Anwendungen* (Berlin: Springer-Verlag, 1981); Translated into English: *Cryopumping. Theory and Practice* (Oxford: Clarendon Press, 1989); Translated into Russian: *Kriovakuumnaya Tekhnika. Osnovy i Primeneniya* (Moscow: Energoatomizdat, 1983)
76. Labuntsov D A, Yagov V V *Mekhanika Dvukhfaznykh Sistem* (Mechanics of Two-Phase Systems) (Moscow: Izd. MEI, 2000)
77. Rose J, in *Proc. of the 11th Intern. Heat Transfer Conf., 23–28 August 1998, Kyongji, Korea* Vol. 1 (Seoul: Korean Society of Mechanical Engineers, 1998) p. 89
78. Rose J W *Proc. R. Soc. Lond. A* **411** 305 (1987)
79. Mills A F, Seban R A *Int. J. Heat Mass Transfer* **10** 1815 (1967)
80. Kryukov A P et al. *J. Vac. Sci. Technol. A* **24** 1592 (2006)
81. Kryukov A P, Levashov V Yu, Shishkova I N *J. Eng. Phys. Thermophys.* **78** 639 (2005); *Inzh.-Fiz. Zh.* **78** (4) 15 (2005)
82. Aristov V V, Cheremisin F G *Pryamoe Chislennoe Reshenie Kineticheskogo Uravneniya Bol'tsmana* (Direct Numerical Solution of the Boltzmann Kinetic Equation) (Moscow: Vychislitel'nyi Tsentr RAN, 1992)
83. Aoki K, Takata S, Kosuge S *Phys. Fluids* **10** 1519 (1998)
84. Kryukov A P, Levashov V Yu, Shishkova I N *J. Appl. Mech. Tech. Phys.* **45** 407 (2004); *Prikl. Mekh. Tekh. Fiz.* **45** (3) 119 (2004)
85. Levashov V Yu, Kryukov A P, Shishkova I N *Int. J. Heat Mass Transfer* **127** 115 (2018)
86. Sone Y, Aoki K, Yamashita I, in *Proc. of the 15th Intern. Symp. on Rarefied Gas Dynamics* Vol. II (Eds V Boffi, C Cercignani) (Stuttgart: B.G. Teubner, 1986) p. 323
87. Kryukov A P, Levashov V Yu *High Temp.* **46** 700 (2008); *Teplofiz. Vys. Temp.* **46** 765 (2008)
88. Isachenko V P *Teploobmen pri Kondensatsii* (Heat Exchange during Condensation) (Moscow: Energiya, 1977)
89. Taguchi S, Aoki K, Takata S *Phys. Fluids* **15** 689 (2003)
90. Pong L, Moses G A *Phys. Fluids* **29** 1796 (1986)
91. Panzarella C, Kassemi M *Int. J. Heat Mass Transfer* **52** 3767 (2009)
92. Mouratova T M *Int. J. Heat Mass Transfer* **16** 1407 (1973)
93. Muratova T M *Izv. Akad. Nauk SSSR. Energetika Transport* (6) 140 (1980)
94. Toei R et al. *J. Chem. Eng. Jpn.* **1** 125 (1968)
95. Shankar P N, Deshpande M D *Phys. Fluids A* **2** 1030 (1990)
96. Persad A H, Ward C A *Chem. Rev.* **116** 7727 (2016)
97. Ward C A, Fang G *Phys. Rev. E* **59** 429 (1999)
98. Kryukov A P, Levashov V Yu, in *Tr. XIV Minsk. Mezhdunar. Foruma po Teplo- i Massoobmenu, 10–13 Sentyabrya 2012 g.* (Proc. of the 14th Minsk Intern. Congress on Heat Exchange, September

10–13, 2012) Vol. 2 (Minsk: Inst. Teplo- i Massoobmena NAN Belarusi, 2012) p. 42
99. Frezzotti A *Phys. Fluids* **23** 030609 (2011)
100. Frezzotti A, Barbante P *Mech. Eng. Rev.* **4** (2) 16 (2017)
101. Kon M, Kobayashi K, Watanabe M *Phys. Fluids* **26** 072003 (2014)
102. Kon M, Kobayashi K, Watanabe M *Eur. J. Mech. B* **64** 81 (2017)
103. Shishkova I N, Kryukov A P, Levashov V Yu *Int. J. Heat Mass Transfer* **112** 926 (2017)
104. Struchtrup H, Frezzotti A, in *Book of Abstracts of the 31st Intern. Symp. on Rarefied Gas Dynamics, Glasgow, UK, July 23–27, 2018* (Eds Y Zhang et al.) (New York: AIP, 2018) p. 274
105. Zhakhovskii V V, Anisimov S I *J. Exp. Theor. Phys.* **84** 746 (1997); *Zh. Eksp. Teor. Fiz.* **111** 1328 (1997)
106. Anisimov S I, Dunikov D O, Zhakhovskii V V, Malyshenko S P *J. Chem. Phys.* **110** 8722 (1999)
107. Zhakhovsky V V et al. *Proc. Natl. Acad. Sci. USA* **116** 18209 (2019)
108. Zhakhovskii V V, Zybin S V, Nishihara K, Anisimov S I *Phys. Rev. Lett.* **83** 1175 (1999)
109. Matsumoto M, Yasuoka K, Kataoka Y *Fluid Phase Equilib.* **104** 431 (1995)
110. Tsuruta T, Tanaka H, Masuoka T *Int. J. Heat Mass Transfer* **42** 4107 (1999)
111. Matsumoto M *Fluid Phase Equilib.* **125** 195 (1996)
112. Matsumoto M *Fluid Phase Equilib.* **144** 307 (1998)
113. Anisimov S I, Zhakhovskii V V *JETP Lett.* **57** 99 (1993); *Pis'ma Zh. Eksp. Teor. Fiz.* **57** 91 (1993)
114. Gibelli L, Lockerby D, Sprittles J, in *Book of Abstracts of the 31st Intern. Symp. on Rarefied Gas Dynamics, Glasgow, UK, July 23–27, 2018* (Eds Y Zhang et al.) (New York: AIP, 2018) p. 82
115. Watanabe C et al., in *Book of Abstracts of the 31st Intern. Symp. on Rarefied Gas Dynamics, Glasgow, UK, July 23–27, 2018* (Eds Y Zhang et al.) (New York: AIP, 2018) p. 301
116. Bird E, Liang Z *Phys. Rev. E* **100** 043108 (2019)
117. Lu Z et al. *IEEE Trans. Compon. Packag. Manufact. Technol.* **6** 1056 (2016)
118. John B et al. *Phys. Rev. Fluids* **4** 113401 (2019)
119. Kryukov A P, Levashov V Yu, Pavlyukevich N V *J. Eng. Phys. Thermophys.* **87** 237 (2014); *Inzh.-Fiz. Zh.* **87** (1) 229 (2014)
120. Kryukov A P, Levashov V Y *Heat Mass Transfer* **52** 1393 (2016)
121. Nakamura S, Yano T, in *Book of Abstracts of the 31st Intern. Symp. on Rarefied Gas Dynamics, Glasgow, UK, July 23–27, 2018* (Eds Y Zhang et al.) (New York: AIP, 2018) p. 206
122. Fang G, Ward C A *Phys. Rev. E* **59** 417 (1999)
123. Frezzotti A, in *Book of Abstracts of the 31st Intern. Symp. on Rarefied Gas Dynamics, Glasgow, UK, July 23–27, 2018* (Eds Y Zhang et al.) (New York: AIP, 2018) p. 75
124. Shishkova I N, Kryukov A P, Levashov V Yu *Int. J. Heat Mass Transfer* **141** 9 (2019)
125. Borodulin V Yu et al. *Int. J. Heat Mass Transfer* **109** 609 (2017)